ACTIVE FIBER BRAGG GRATING FLOW SENSOR POWERED BY IN-FIBER LIGHT

by

Lucas J. Cashdollar

B.S. in Electrical Engineering, University of Pittsburgh, 2002

Submitted to the Graduate Faculty of

The School of Engineering in partial fulfillment

of the requirements for the degree of

Master of Science

University of Pittsburgh

2004

UNIVERSITY OF PITTSBURGH

SCHOOL OF ENGINEERING

This thesis was presented

by

Lucas J. Cashdollar

It was defended on

September 3, 2004

and approved by

Dr. Joel Falk, Professor, Electrical Engineering

Dr. Dietrich W. Langer, Professor, Electrical Engineering

Dr. Kevin P. Chen, Paul E. Lego Assistant Professor, Electrical Engineering

ACTIVE FIBER BRAGG GRATING FLOW SENSOR POWERED BY IN-FIBER LIGHT

Lucas J. Cashdollar, MS

University of Pittsburgh, 2004

Tunable fiber Bragg gratings (FBGs) are key components for optical communications and sensing applications. Current tuning mechanisms include on-fiber electric heating, the piezo-electric effect, and mechanical stretching and bending. Unfortunately, all of these tuning mechanisms rely on external electrical power supplied by non-optical means. Additional electrical cabling increases manufacturing cost and the risks of failure associated with additional on-fiber electrical contacts and fragile packaging, which are susceptible to electromagnetic interference. These limitations make current fiber components no longer suitable for use in hostile environments, such as extreme temperature, corrosive, and humid environments.

The research herein presents a tunable fiber Bragg grating device without sophisticated packaging and external electrical wiring. Shown for the first time, the resonance wavelength, spectrum width, and chirp can be directly controlled by in-fiber light as well as spectral responses of metal-coated fiber Bragg gratings. In-fiber diode laser light at 910-nm was leaked from the fiber and absorbed by the surrounding metallic coating to raise the grating's temperature and to change the background refractive index distribution of the gratings. Wide tunability of the resonance wavelength and spectral width was demonstrated in both uniform and linear chirped gratings.

Applications of in-fiber light-powered active grating sensors are demonstrated for dual function temperature and flow sensors based on self-heated optical hot wire anemometry. A grating flow sensor has been experimentally evaluated for different grating lengths and input laser powers. The grating flow sensor demonstrated a minimum measurable flow velocity for nitrogen gas flow of 0.35-m/s at atmosphere pressure, which is comparable to or better than most MEMS-based flow sensors.

Optical fiber is not used only for optical signal delivery, but also as a multi-function cable that can deliver optical power for on-fiber self-heating. This one-fiber solution provides a new dimension to designing multifunctional fiber sensors without compromising their intrinsic advantages, which include immunity to electromagnetic fields, low cost, long lifetime, and the capability to function in harsh environments.

TABLE OF CONTENTS

LIST OF TABLES

LIST OF FIGURES

ACKNOWLEDGEMENTS

I would like to thank numerous people for their support during my graduate work at the University of Pittsburgh. Without their help the work presented in this thesis would not have been possible. First, I would like to thank my advisor and supporter Dr. Kevin P. Chen for being patient with and teaching his first graduate student who, at the start of his graduate studies, had no real knowledge of optical electronics. I am grateful for the amount of theory and accompanying equipment/technology that Dr. Chen has taught me. And I would like to thank Dr. Joel Falk for allowing me to have a work space in his lab.

Also, I would like to thank Dr. Marlin H. Mickle and his students, Dan Ulinski, Carl Taylor, Randy Maruschock, and Dan Harrist for alternate guidance and technical support. I would like to thank Jim Lyle for technical support and put out a special thanks to Jim Stango for helping out with equipment even after I had moved on from being employed at the University of Pittsburgh's Physics and Astronomy Department. If it was not for Sandy Weisberg I may have forgotten to graduate among many other things. Special thanks go out to Steve Hackworth and Josh Ferris for finding the time to do a last minute proofread of my thesis before the dissertation committee's submission deadline. Finally, I would like to thank my family for keeping me going all these years.

1.0 INTRODUCTION

1.1 MOTIVATION

Invented in the late 1970s, fiber Bragg gratings were recognized for their importance in fiber optic communication systems and sensing[1, 2]. Fiber Bragg gratings (FBGs) are simple optical devices formed by periodic modulations in the refractive index along the length of the device (z-axis), which are induced by UV laser radiation. The basic operation of the fiber Bragg grating is illustrated in Figure 1.1. Light sent down a fiber containing a grating will reflect light back only at a certain wavelength, the Bragg wavelength (λ_B), which is a function of the period of the periodic change of the device's index of refraction (Λ) and the effective index of the fiber core (n_{eff}), as shown in the following equation:

$$\lambda_B = 2n_{eff}\Lambda \tag{1-1}$$

Bragg grating components have applications in wavelength filtering [3-5], routing [6], dispersion compensation [7, 8], and fiber sensing. Over the past decade much research has been dedicated to understanding the fundamental mechanisms behind grating fabrication and the development of new grating applications. In-fiber components offer several important advantages over other optical and electronic components. Such advantages include, but are not limited to, low manufacturing cost and long life time, immunity to electromagnetic fields, high sensitivity, and the capability of functioning for extended periods of time in harsh environments. Due to the small size and low transmission loss of fiber Bragg gratings allow for the deployment of sensor

arrays for use in multipoint long distance remote sensing. By chaining multiple sensors together it is possible to develop multi-point strain/temperature monitoring systems for smart structures [9] and medical applications [10]. Also, many innovative FBG sensors have been reported, which are based on the index of refraction temperature and stress induced effects, such as acoustic, pressure, tilt, and acceleration sensors [11-14].

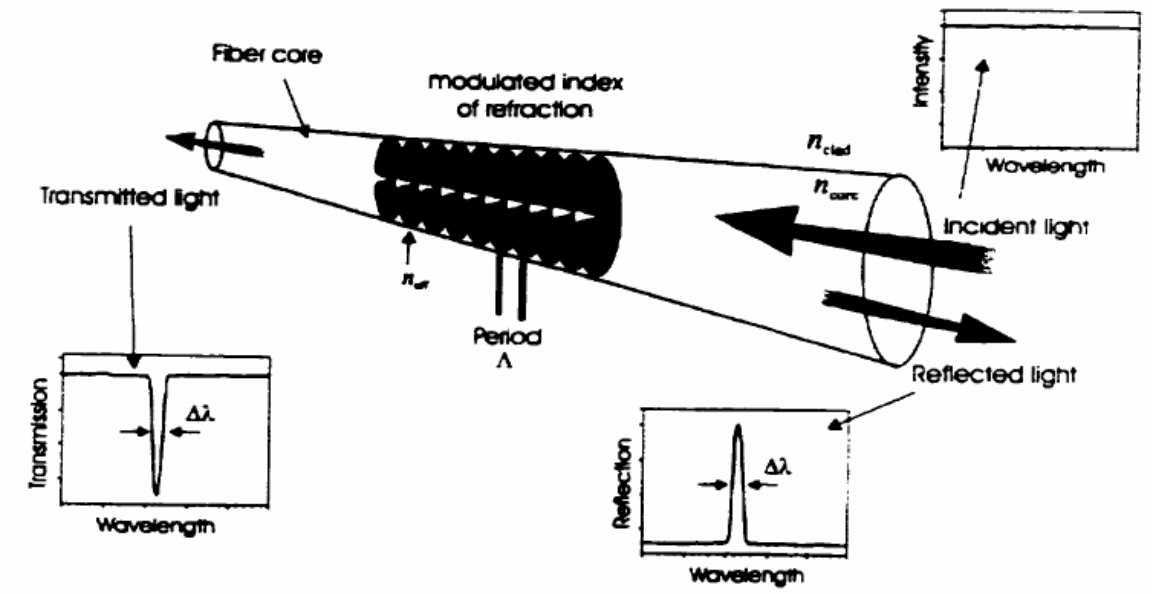

Figure 1.1: Basic operational schematic for a fiber Bragg grating[15].

Although the inherent advantages of in-fiber optical components are promising, their applications have been limited due to their total passivity. Fiber Bragg gratings are sensitive to external changes, such as changes in temperature and/or applied strain. These external forces change the device's index of refraction, which in turn alter the grating's physical parameters. Bulky electro/mechanical devices are required to eliminate effects of temperature-drifting, allow network components to be reconfigured, and change sensing parameters such as sensitivity, set points, triggering time, dynamic range, and responsivity[16]. By controlling the parameters

mentioned above the functionality of FBGs has been increased by the addition of tuning mechanisms. Over the past few years a number of tuning mechanisms have been created, such as on-fiber electrical heating [3, 8, 17-19], bending and stretching due to the piezoelectric effect [7, 20], mechanical bending and stretching [21, 22], and acoustic modulation [5]. Goh *et al.* were able to tune 90 nm by mechanical stretching and bending. Also, dynamic chirp gratings used for dispersion compensation by controlling the chirp of the grating have been demonstrated [7, 8].

Although the advantages of tunable fiber Bragg grating components are obvious a few common drawbacks for active fiber components still exist. The drawbacks for active fiber optical components include the need to have electrical power and control signals delivered to actuators, resistive coatings, etc., via electrical cabling. The electrical cabling and the fact that the tuning mechanism itself is bulky add to the manufacturing cost of the device and limit the device's ability to be embedded for uses such as monitoring for smart structures. Also due to the cabling, the device is no longer immune to electrical interference, the device's lifetime is short in comparison to the silica fiber Bragg grating, and the device is not suitable for use in hostile environments, such as humid and/or corrosive environments, high-g overload, or strong electromagnetic interference.

Dr. Kevin P. Chen of University of Pittsburgh has developed a method to deliver the power and control signals necessary for active fiber Bragg grating devices via in-fiber diode laser light[16]. The power and control signals for active fiber Bragg grating components are sent down the fiber by light, thus eliminating the need for external electrical cabling. The tuning mechanism powered and controlled by in-fiber light is shown in Figure 1.2. Light from a multimode fiber, which is fused to a single mode fiber, leaks out into the cladding of the single

mode fiber due to the mode mismatch. The leaking laser light is absorbed by a metallic coating along the length of the grating, which raises the temperature, and can be used to change the physical and optical characteristics of the fiber device by increasing or decreasing the amount of laser light leaked out.

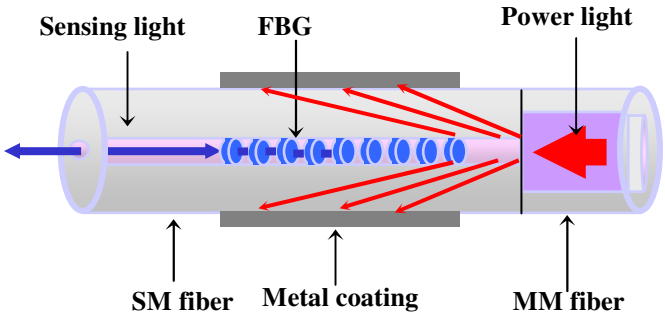

Figure 1.2: Schematic of a active in-fiber grating sensor powered by in-fiber light.

The motivation of this thesis is to build upon the concept of fiber Bragg gratings powered by in-fiber light by exploring a fiber optic sensor that is powered by in-fiber light where the light was extracted by the localized light absorber and converted into thermal energy. The results herein present the development and specifications of an active fiber Bragg grating flow sensor, based on hot wire anemometry. To the author's knowledge, a passive fiber Bragg grating flow sensor does not currently exist, due to the large amount of air flow needed to result in a noticeable spectral response. A passive flow sensor, based hot wire anemometry, would have an impractical spectral response due to the 1-nm/70ºC responsivity of the device[15]. The active flow sensor presented in this work, however, overcomes the shortcomings inherent in a passive FBG flow sensor, since the in-fiber light can heat the grating considerably so that a small flow results in a large amount of heat dissipation. Therefore, a small amount of air flow on the order of hundreds of milliliters per second can cause a noticeable change in the reflectance spectra.

The active flow sensor powered by in-fiber laser light is comparable to other fiber optical and MEMS based flow sensors and has a comparable minimum flow velocity of 0.35 m/s.

1.2 THESIS ORGANIZATION

Chapter 2 contains the background information of the thesis and begins with a brief history of fiber Bragg gratings followed by a section on photosensitivity, physics, and fabrication techniques. Two models based on the effects of the "wrong bonds" or germanium oxygen deficient centers, thought to be what causes photosensitivity, will be discussed, which include the color center model and the compaction model. The basic physics of fiber Bragg gratings, including index modulation, reflectivity, bandwidth, and grating dependency on both temperature and strain will also be discussed. Four grating fabrication methods will be presented, which include internal writing, point-by-point, interferometric, and the phase mask techniques

Chapter 3 contains the experimental setup and characterization techniques for fiber Bragg grating fabrication, which utilizes the phase mask fabrication technique. The optical setup, fiber to phase mask alignment procedure, *in-situ* monitoring techniques for grating inscription, and typical spectra responses of gratings inscribed using this fabrication system will be discussed in detail.

Chapter 4 introduces the concept of tunable fiber Bragg gratings. Various tuning mechanisms will be discussed, such as mechanical and electrical methods, and the in-fiber laser light tuning mechanism, developed by Dr. Kevin P. Chen *et al*., will be presented, with experimental results.

Chapter 5 introduces an active fiber Bragg grating dual temperature and flow sensor powered by in-fiber diode laser light. The sensor is based on hot wire anemometry. The sensor design, experimental setup, and results will be discussed.

Chapter 6 contains the conclusion and summary for the work presented in this thesis, as well as a list of publications resulting from this work. The chapter also contains a section on possible future work that will expand on the work presented in Chapter 4, increasing the range and flexibility of in-fiber tuning by utilizing a specialty double clad fiber.

2.0 FIBER BRAGG GRATINGS

The Fiber Bragg Grating was first developed in 1978 by K.O. Hill *et al.* at the Canadian Communication Research Center [1]. By beaming 488-nm light from an Argon laser into a one meter long photosensitive germanium doped silica fiber caused a periodic change in the index of refraction within the core of the fiber. The laser light interfered with the Fresnel reflected beam that resulted from the 4% of the laser light being back reflected from the fiber's cleaved end. This interference created a weak standing wave pattern. The varying intensity of the standing wave pattern changed the index of refraction of the photosensitive fiber [1, 23]. The grating fabrication process, which Hill and associates used, was called the internal writing technique [15].

The grating fabricated by Hill *et al.* was instantly recognized useful in telecommunications applications, but was limited due to the reflection wavelength of the grating only being in the visible part of light spectrum. By using the internal writing technique to fabricate a grating the wavelength of the reflected light was the same as the wavelength used to write the grating. Over a decade later, a fabrication method was introduced which eliminated the wavelength limitations of the fiber Bragg grating. Meltz *et al.* using an Excimer laser produced a two beam 244-nm UV interference pattern on the side of a Ge-Silica fiber and were able to write a grating [24]. By changing the angle between the interference beams, the wavelength at which the grating was fabricated was able to be shifted to more useful points within the light spectrum, such as one of the three telecom windows. The period of the index of refraction modulation can be varied to produce a desired reflection wavelength.

Building upon the Interferometric fabrication technique devised by Meltz *et al.*, Kashyap and associates were able to fabricate fiber Bragg gratings at the telecom wavelength of 1530-nm [25]. This breakthrough allowed the realization of fiber Bragg gratings being used as wavelength multiplexers and passive wavelength filters for telecommunication applications [25].

2.1 OPTICAL FIBER PHOTOSENSITIVITY

Photosensitivity was first discovered in 1978 when K. O. Hill *et al.* accidentally created the first fiber Bragg grating by modulating the index of refraction of a germaniumsilica fiber using high intensity argon laser light. Photosensitivity can be thought of as the measure of the amount of index change caused when a grating is written. Major research into photosensitivity did not occur for about a decade due to researchers believing that the fiber used by Hill was a specialty fiber that was not readily available[23]. However, in 1989 when Meltz *et al.* developed a simple grating fabrication method, the interferometric technique, major research once again began, since the grating fabrication process was simplified.

Defects in germanium doped silica fiber are generally accepted as the cause of the photosensitivity phenomenon[15]. These defects are referred to as germanium oxygen-deficient centers (GODCs). When germanium bonds with silica during the fiber manufacturing process one germanium atom bonds to four silica atoms via oxygen, but sometimes Ge-Si or Ge-Ge "wrong bonds" occur, these defects cause the fiber to be photosensitive. When light of wavelength ranging from 240 to 250 nm is applied to the fiber, more defects are created, which are called GeE' centers, and free electrons are released. The released electrons can recombine with Ge molecules or move on through the glass matrix and combine at Ge(1) and Ge(2) centers (missing an electron) to form $Ge(1)^-$ and $Ge(2)^-$ defect sites, where the number in parentheses

refers to the number of neighboring Si molecules, see Figure 2.1. These newly created deficiency sites now have a different absorption wavelength, which cause the changes in the index of refraction of the fiber. Photosensitivity has been reported at wavelengths other than the 240 to 250-nm range, such as 157, 193 and 260 nm, which implies that other wavelengths are absorbed by the defect sites[26].

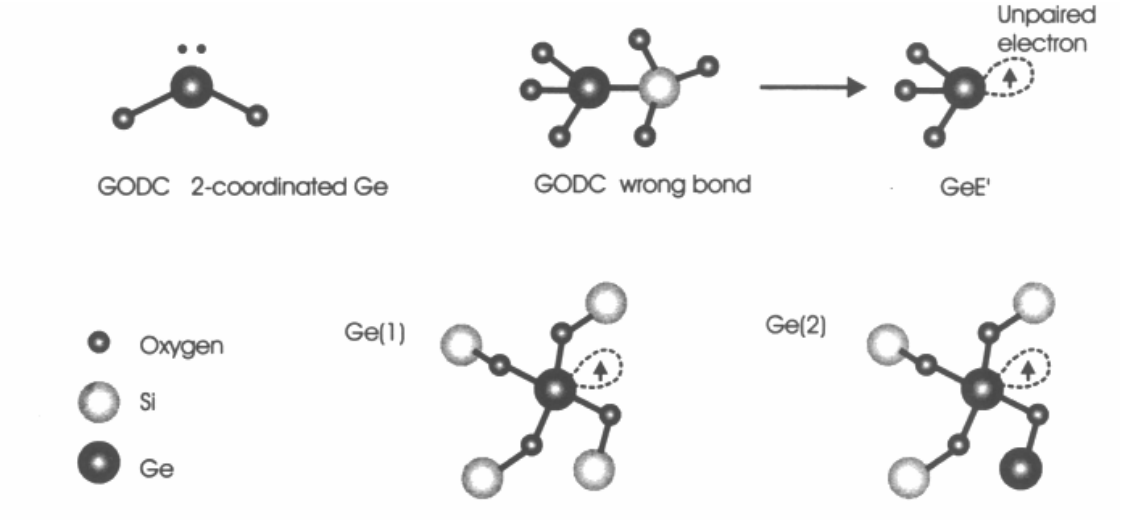

Figure 2.1: Molecular representation of the defects in germanium doped silica fiber, the top shows the "wrong bond" and GeE' defects, and the bottom shows the Ge(1) and Ge(2) color centers[15].

Two models based on the effects of the "wrong bonds" or germanium oxygen deficient centers will be discussed, which include the color center model and the compaction model. The color center model is based on the idea that photo-induced changes in the absorption spectrum of the material cause a change in the index of refraction of the material. The compaction model is based on the density changes caused in the material by the incoming laser radiation, which changes the index of refraction accordingly.

Based on the color model, when UV radiation is absorbed the "wrong bonds" free electrons which in turn create $Ge(1)^-$ and $Ge(2)^-$ defect sites with associated absorption bands. The Kramers-Kronig relation as found in Reference 27:

$$\varepsilon_r(\lambda) = 1 + \int \frac{\varepsilon_i(\lambda')}{\lambda' - \lambda} d\lambda' \tag{2-1}$$

relates the real and imaginary parts of the complex dielectric constant (ε), which allows for the absorption and refractive index of the material to be plotted, see Figure 2.2(a) [27, 28]. Figure 2.2(b) shows the color change of a grating along the z-axis of a fiber, written at 157 nm using an ArF laser[29].

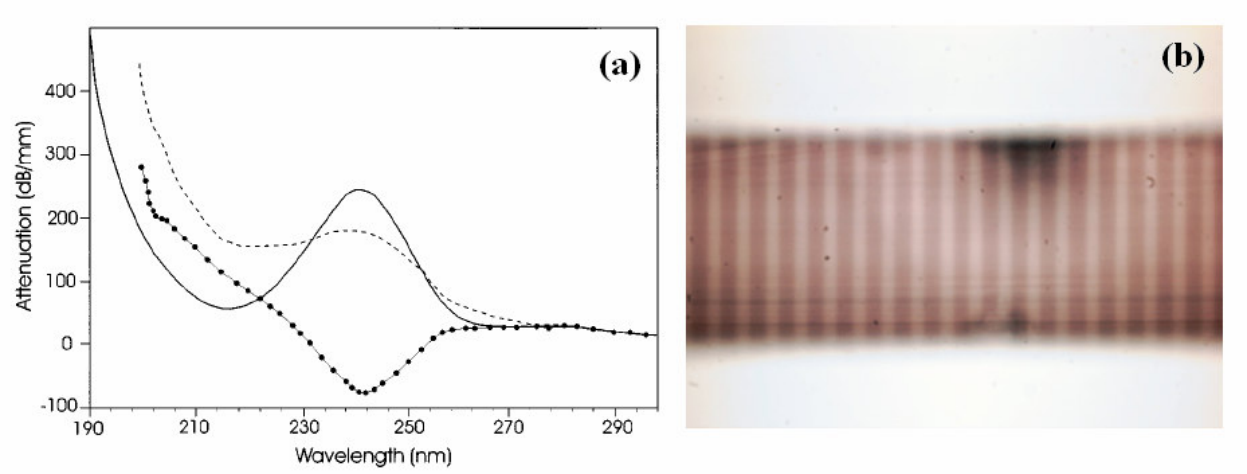

Figure 2.2: (a) UV absorption spectra before (solid line) and after (dashed line) writing a 81% peak reflectivity grating in an AT&T Accutether single-mode fiber. The squares denote the change in attenuation[28] (b) color change of a grating along the z-axis of a fiber written at 157 nm[29].

The compaction model is based on the relationship between the density of the material in question and the index of refraction, which is shown in the differentiation of the Lorenz-Lorenz equation as found in Reference 30, which gives the following:

$$\Delta n = \frac{(n^2 - 1)(n^2 + 2)}{6n^2}\left(\frac{\Delta\alpha}{\alpha} - \frac{\Delta V}{V}\right) \tag{2-2}$$

where the values $\Delta\alpha$ and ΔV are the relative changes in the electric polarizability and volume of the material, respectively. Figure 2.3 shows a plot of the observed compaction of an initially 100-nm thick silica film as a function of 248-nm UV dose (open circles). The solid square represents the evolution of the refractive index change versus an accumulated UV dose. The refractive index of the material decreased by 0.5 with an accumulated does of 10^4 Joule/cm^2. The solid circles represent the restoration of the original film thickness by annealing the material for an hour at 950ºC[30].

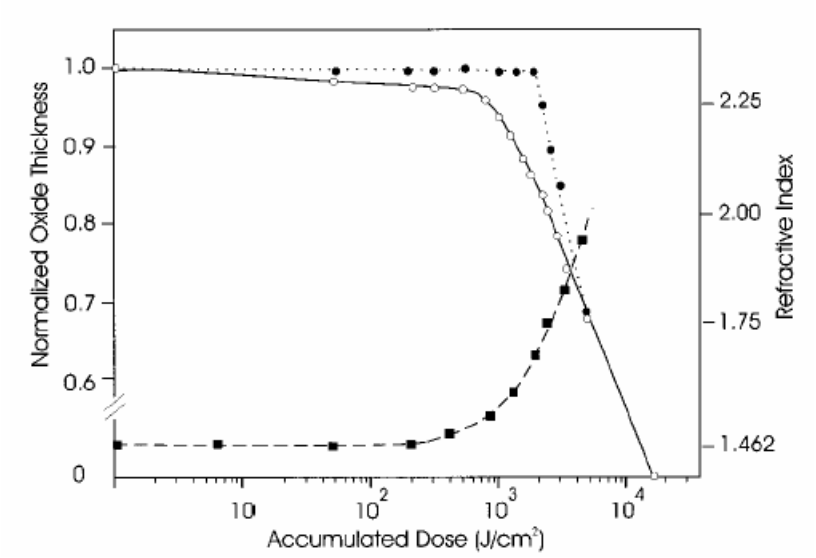

Figure 2.3: Observed compaction of an initially 100-nm thick silica film as a function of 248-nm UV dose (open circles), refractive index change versus an accumulated UV dose (solid squares), and restoration of the original film thickness by annealing the material for an hour at 950ºC[28].

The photosensitivity of optical fiber can be enhanced by a number of processes, which include increasing the germanium dopant in germaniumsilica fiber, hydrogen loading, and flame brushing. The methods mentioned above, excluding an increase in the amount of germanium dopant, were devised to eliminate the poor coupling between telecommunications fiber of different core indexes. For instance, the loss between two fusion spliced 4% germanium doped

fibers was found to be about 0.1 dB whereas the loss between 4% and 8% doped fiber was on the order of 1 dB.

By increasing the amount of germanium dopant in the core of a silica fiber the photosensitivity of the fiber increases. The following fibers doped with 4% (standard fiber), 10%, and 20% of germanium exhibit a saturated index modulation of $3.4x10^{-5}$, $5x10^{-4}$, and $2.5x10^{-4}$, respectively[15]. The majority of the research presented in this thesis uses 8% germanium doped silica fiber, which has twice the dopant of standard telecom fiber.

By hydrogenation, the process of soaking fiber in hydrogen gas, the saturated index modulation of the fiber can be increased up to 0.01, or typically an order of magnitude higher than the index change caused in plain germanium doped fiber. The hydrogenation process is as follows: germanium doped or germanium free fiber is placed into a chamber pressurized typically at 150 atm with hydrogen gas at room temperature[15], usually for about two weeks. The time needed to diffuse hydrogen into standard fiber can be decreased to about 2 days if the chamber is heated to a temperature of approximately 150ºC. Once the hydrogenated fiber has been written the index change in the fiber becomes permanent and the background hydrogen not exposed to the UV light diffuses out. By diffusing hydrogen into the fiber the hydrogen reacts with the Ge-O-Si molecules to form Ge deficiency centers and free OH molecules, therefore increasing the photosensitivity of the fiber when UV light at roughly 240-nm is applied[28]. A drawback to hydrogenated fiber is that the hydrogen diffuses out of the fiber over time unless refrigerated (~-40ºC) and if the loading setup is not properly installed a high risk of catastrophe can result. Another disadvantage is that the OH molecules, formed when the deficiency centers are created, result in a large absorption at the telecom wavelengths of 1.39 and 1.41 μm, which results in large signal attenuation[28].

The flame brushing technique is similar to hydrogen loading, but the hydrogen is applied using a hydrogen fueled flame that is brushed along the length of fiber in question. The flame reaches a temperature of about 1700ºC, which weakens the fiber. The index change is an order of magnitude higher than that of standard germanium doped fiber ($\Delta n \sim 10^{-3}$)[28].

Table 2.1 shows the reflectivity of a 1.5-mm grating written into a variety of fibers enhanced by various techniques. Each fiber has a known concentration of germanium and was written for a known time.

Table 2.1: Comparison of various fibers and enhancements by various techniques [28]

Fiber type	GeO_2 in fiber core mol %	Reflectivity of 1.5 mm Bragg grating %	Time required to inscribe the grating
Philips, matched cladding	5	17	60 min
Philips, depressed cladding	4	20	60 min
Deeside fiber	5	17	60 min
Corning payout fiber	8	29	90 min
Hydrogenated standard fiber	4	60	10 min
High index fiber	20	77	10 min
Reduced fiber	12	97	5 min
Boron codoped	17	91	1 min
Hydrogenated boron-codoped fiber	17	87	10 s

The fiber used to created the gratings used in the research presented in this thesis was standard (125/65-μm) 8% doped germaniumsilica fiber.

2.2 FBG PHYSICS

The information presented herein will focus on the basic physics of fiber Bragg gratings, covering index modulation, reflectivity, bandwidth, and grating dependency on temperature and

strain. Theoretical plots of reflectivity for two different length gratings will be presented which shows that the reflective strength of the grating depends on the length of the gratings and index modulation amplitude. All theoretical plots are based on the fiber parameters for the Corning SMF-28 single mode standard telecommunications fiber doped with 4% Germanium.

2.2.1 Index Modulation and Reflectivity

The periodic modulation change of the index of the fiber along the z-axis creates a grating in the fiber, known as a Bragg grating. A uniform Bragg grating is a simple FBG where the period of modulation and amplitude of the index change is held constant for the entire length of the fiber. The index modulation profile can be calculated with[15]:

$$n(z) = n_{avg} + \Delta n \cos\left(\frac{2\pi z}{\Lambda}\right) \tag{2-3}$$

where n_{avg} is the average refractive index of the core of the fiber and Δn is the amplitude of the periodic index change [15]. The average index of refraction of the fiber core can be calculated using the following formula[29]:

$$n_{avg} = \frac{1}{2}(\Delta n) + n_{core} \tag{2-4}$$

where n_{core} is the index of the fiber core. Shown in Figure 2.4 is a graphical representation of the index modulation of a grating letting n_{core} = 1.486, $\Delta n = 10^{-4}$, and the Bragg period equal to 5.28×10^{-7}, which corresponds to a Bragg wavelength of 1550nm when the effective index is 1.4862.

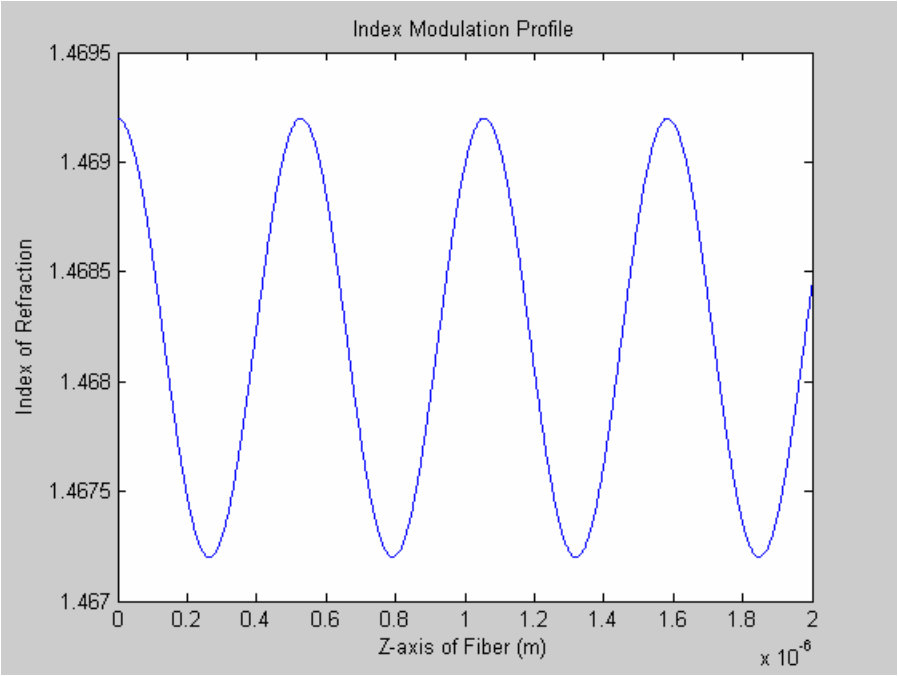

Figure 2.4: The Index Modulation Profile along the z-axis of the fiber Bragg grating

The reflectivity of the grating can be calculated using the following formula[15], which is a function of the wavelength of the incident light, λ, and the grating length l:

$$R(l,\lambda) = \frac{\Omega^2 \sinh^2(sl)}{\Delta k^2 \sinh^2(sl) + s^2 \cosh^2(sl)} \tag{2-5}$$

Where $\Delta k = 2\pi n_{avg}/\lambda - \pi/\lambda$ and $s = (\Omega^2 - \Delta k^2)^{1/2}$. The coupling coefficient, Ω, is the index of refraction modulation along the z-axis of the fiber and is found using the following formula[15]:

$$\Omega = \frac{\pi \Delta n}{\lambda} M_p \tag{2-6}$$

M_p is the fraction of the mode power contained by the fiber core and is a function of the V-number, V, where $M_p = 1 - V^{-2}$. The value Δn is the amplitude of the periodic index change in

the grating, which typically should be in the range of 10^{-5} to 10^{-3} times larger than the index of the core.

When the incident light is at the Bragg wavelength, Δk=0 and the Reflectance formula reduces to the following [15]:

$$R(l,\lambda) = \tanh^2(\Omega l) \tag{2-7}$$

Using the values from the specifications sheet for the Corning SMF-28 single mode standard telecommunications fiber doped with 4% germanium, the peak reflectance of the fiber can be determined as a function of either the length of the grating or the amplitude of the index modulation.

The above equations were used to find the peak reflectance of the fiber for a uniform 4-cm grating with varying index modulation (Δn). The fiber core diameter was 8.2 μm and the numerical aperture was 0.14. The peak wavelength was chosen to match the Bragg wavelength of 1550 nm. The V number was found as follows, where (d) was the diameter of the core of the fiber and NA was the numerical aperture:

$$V = \frac{\pi d}{\lambda} NA = \frac{(\pi)(8.2\mu m)}{1550nm}(0.14) = 2.327$$

The fraction of the mode power in the core was found from:

$$M_p = 1 - V^{-2} = 1 - 0.1847 = 0.8153$$

By substituting the fraction of mode power in the core along with the Bragg wavelength into the equation below the coupling coefficient was found.

$$\Omega = \frac{\pi \Delta n}{1550nm}(0.8153) = 1.653x10^6 \Delta n$$

Once the coupling coefficient was found the length was substituted into the simplified Reflectivity equation along with the desired length of the grating.

$$R(l,\lambda) = \tanh^2[(1.653x10^6 \Delta n)(0.04m)] = \tanh^2(6.612x10^4 \Delta n)$$

Figure 2.5(a) is a plot of the reflectivity of a 4-cm fiber Bragg grating versus the index modulation amplitude. Figure 2.5(b) is a plot of the reflectivity of a 4-mm fiber Bragg grating versus the index modulation amplitude. In order to achieve the same reflectivity for two FBGs of different lengths the index modulation amplitude for the shorter grating must be greater than that of the longer grating. The index modulation amplitude can be increased by allowing the grating to be written longer during the fabrication process.

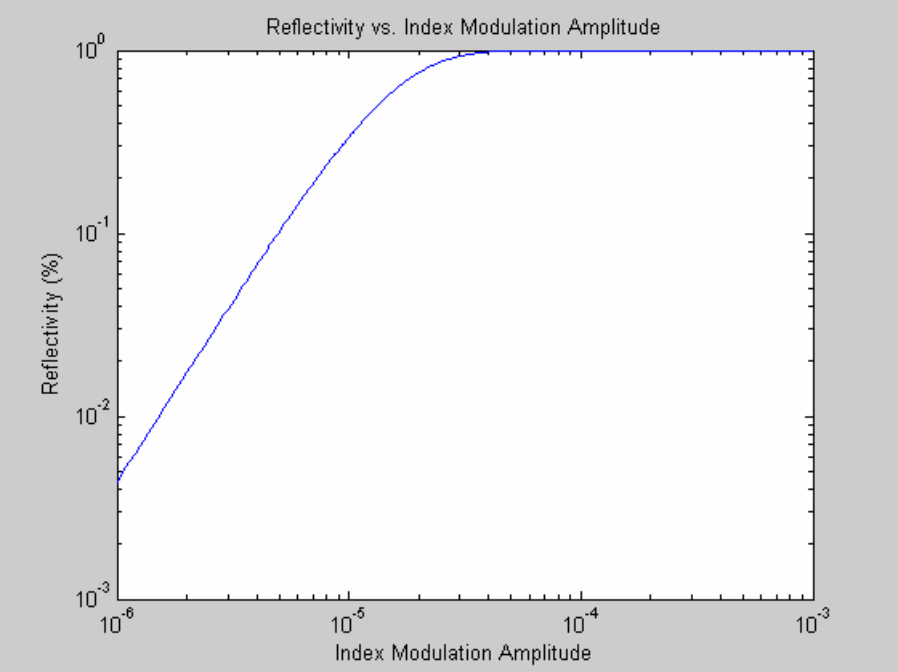

(a)

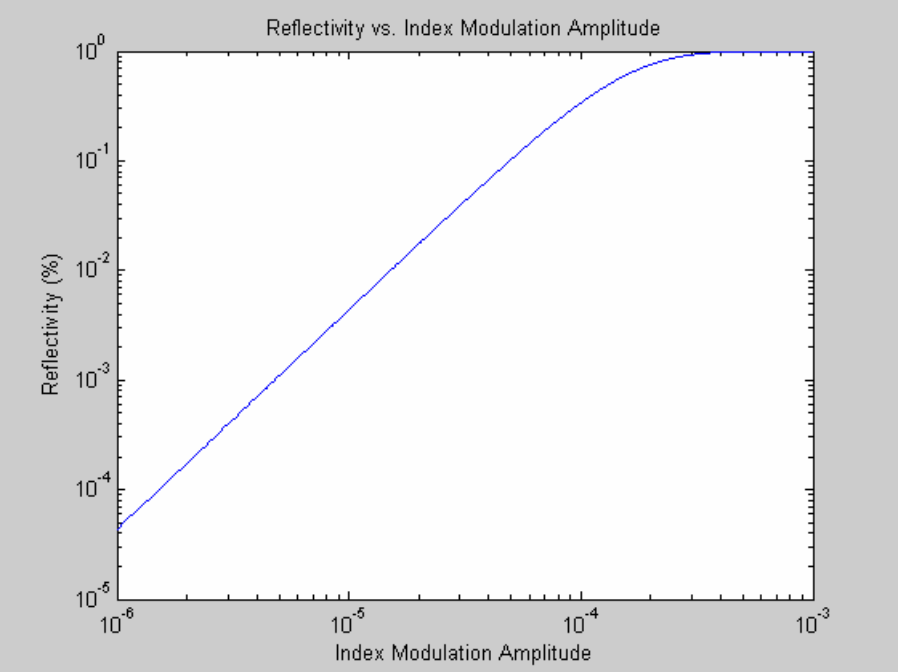

(b)

Figure 2.5: (a) Reflectivity as a function of the index modulation amplitude for a 4-cm grating. (b) Reflectivity as a Function of the index modulation amplitude for a 4-mm grating

By using the graphs in Figures 2.5 (a) and (b) the writing efficiency of a FBG fabrication system can be realized by reading the peak reflection of the recently written grating and finding the corresponding index modulation amplitude.

A typical fiber Bragg grating has a resonance response similar to the one shown in Figure 2.6. The full-width-half-maximum of the grating can be calculated using the following formula:

$$\Delta\lambda = \lambda_B s \sqrt{\left(\frac{\Delta n}{2n_{avg}}\right)^2 + \left(\frac{1}{N}\right)^2} \tag{2-8}$$

where N is the number of grating planes[15]. The FWHM bandwidth of FBGs can be narrowed by increasing the length of the grating.

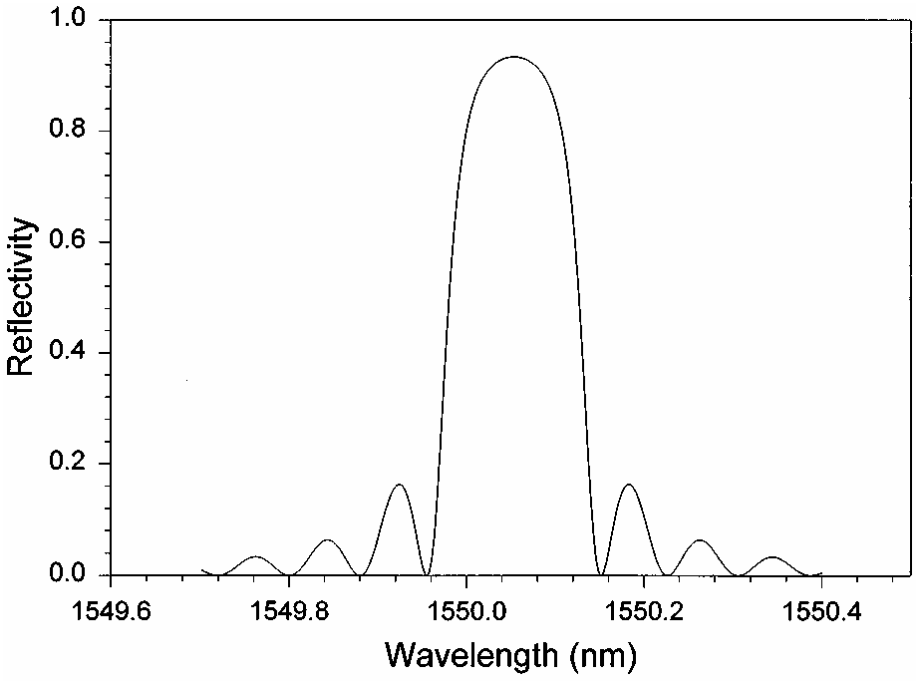

Figure 2.6: Resonance Wavelength for a common fiber Bragg grating[15]

2.2.2 Bragg Grating sensitivity to Temperature and Strain

The index of refraction can be modified by either applied temperature or strain. Temperature and strain also affect the spacing between the grating planes of the FBG. Both of these phenomena result in changing the effective index of refraction for the fiber and the grating spacing, which changes the Bragg wavelength of the device. Therefore, any applied strain or temperature shifts the resonance wavelength and this shift can be measured to calculate the temperature change or amount of strain applied.

The Bragg wavelength shift due to an applied strain is calculated using the following formula[28]:

$$\Delta\lambda_B = \lambda_B(1 - p_e)\varepsilon_z \tag{2-9}$$

where ε_Z is the strain that the fiber is experiencing and is equal to the change in length divided by the original length. The value p_e is known as the effective strain-optic constant and is found as follows[12]:

$$p_e = \frac{n_{eff}^2}{2}[p_{12} - \nu(p_{11} + p_{12})] \tag{2-10}$$

where ν is the Poisson's ratio and p_{11} and p_{12} are the photo-elastic coefficients. For a typical silica fiber p_e is 0.22 [12].

The Bragg wavelength shift due to a change in temperature, ΔT, can be found from the equation below[28]:

$$\Delta\lambda_B = \lambda_B(\alpha_\Lambda + \alpha_n)\Delta T \tag{2-11}$$

where α_Λ is the thermal expansion coefficient and α_n is the thermo-optic coefficient for the fiber. For a typical germanium doped silica fiber the thermal expansion coefficient is

approximately 0.55×10^{-6}/K and the thermo-optic coefficient is approximately 8.6×10^{-6}/K. The index change due to the thermo-optic effect is about sixteen times larger than the index change caused by thermal expansion [15].

The equations for both the strain and temperature effects on the Bragg wavelength follow a linear curve with a constant slope, see Figure 2.7.

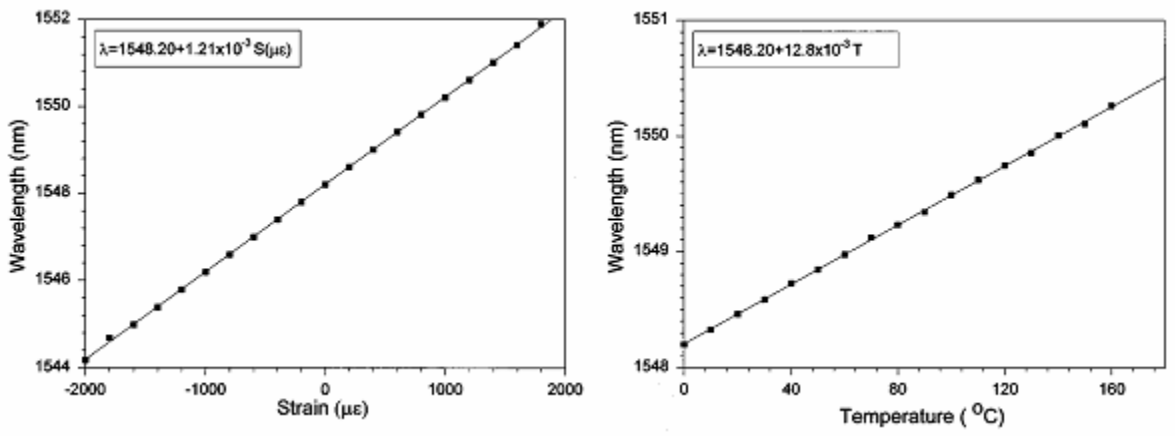

(a) (b)

Figure 2.7: Peak wavelength shift for a Bragg grating under strain (a) and at different temperatures (b) [28].

For a typical germanium silica fiber there was a 1.2-pm change in the peak wavelength due to applying 1-$\mu\varepsilon$ of strain and a 13.7-pm/ºC change for applied temperature[15]. Relying on the fact that fiber Bragg gratings are susceptible to external perturbations useful sensors can be developed. Much research has gone into the development of sensors that can distinguish between the effects of temperature and strain induced wavelength shifts such as a grating tapered FBG cavity sensor and a grating sensor with a Fabry-Perot cavity structure[31, 32].

2.3 GRATING TYPES

Below are descriptions of three typical types of fiber Bragg gratings. The three types are the common Bragg Reflector, blazed Bragg grating, and the chirped Bragg grating.

2.3.1 Common Bragg Reflector

The common Bragg reflector is the most common FBG and was shown in Figure 1.1. The device consists of a periodic modulation of the index of refraction, where the period is held constant. Being the most common type of FBG this grating is used in a majority of applications from sensing to wavelength division multiplexing.

2.3.2 Blazed Bragg Grating

A blazed Bragg grating is a grating where during the writing process the fiber is tilted to create a tilted grating within the core of the fiber. When light hits the tilted grating a portion of the light is leaked out into the cladding of the fiber and eventually out of the fiber. Essentially blazed gratings act as optical taps, see Figure 2.8.

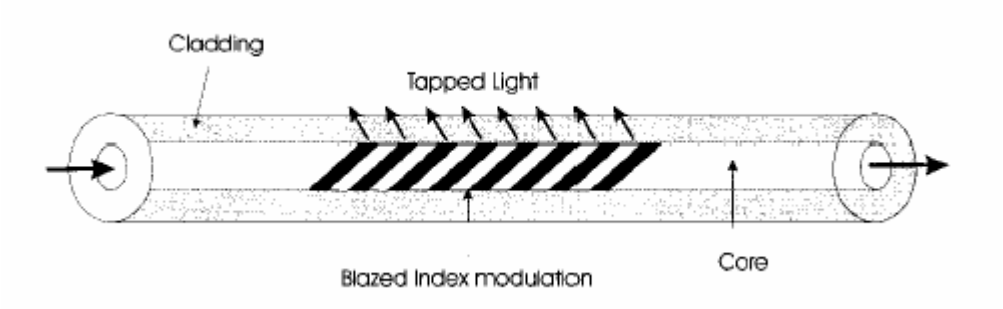

Figure 2.8: Schematic diagram of a Blazed grating[28].

2.3.3 Chirped Bragg Grating

Chirped Bragg gratings differ from common Bragg gratings in that spacing between the grating planes changes monotonically along the z-axis, see Figure 2.9. Chirped gratings are made by either changing the index of refraction profile or the spacing between the grating planes along the z-axis or both. Chirp results in a broadening of the reflected light spectrum. Chirped Bragg gratings are used in dispersion compensation applications.

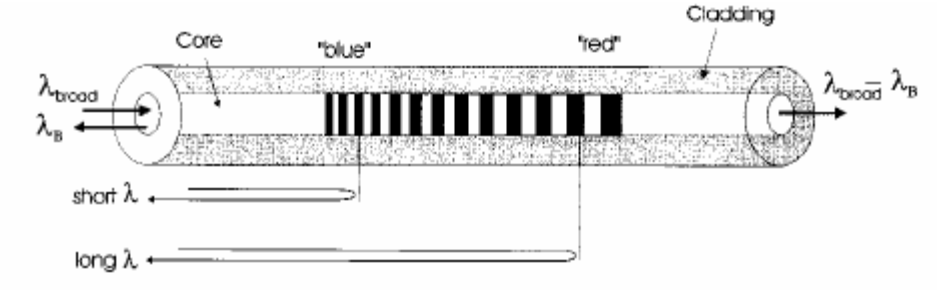

Figure 2.9: Schematic of a chirped Bragg grating showing a uniformly increasing Bragg period along the z-axis of the fiber[28].

2.4 FABRICATION TECHNIQUES

This section describes a few of the fabrications processes used to create fiber Bragg gratings. The four techniques that will be discussed are the internal writing, point-by-point, interferometric, and the phase mask techniques. Some of the methods are discussed for practical reasons and others for historical reasons.

2.4.1 Internal Writing Technique

The internal writing technique was first developed by Hill and coworkers and was used to fabricate the first FBG. Shown in Figure 2.10 was the original setup used by Hill *et al*. [1]. An argon laser was used to send 488-nm light down a one meter piece of Germanium fiber. The incoming laser light interfered with the 4% of the back reflected light from the cleaved end of the fiber to form a standing wave pattern with a periodicity matching that of the argon laser light, which caused a change in the index of refraction of the photosensitive fiber.

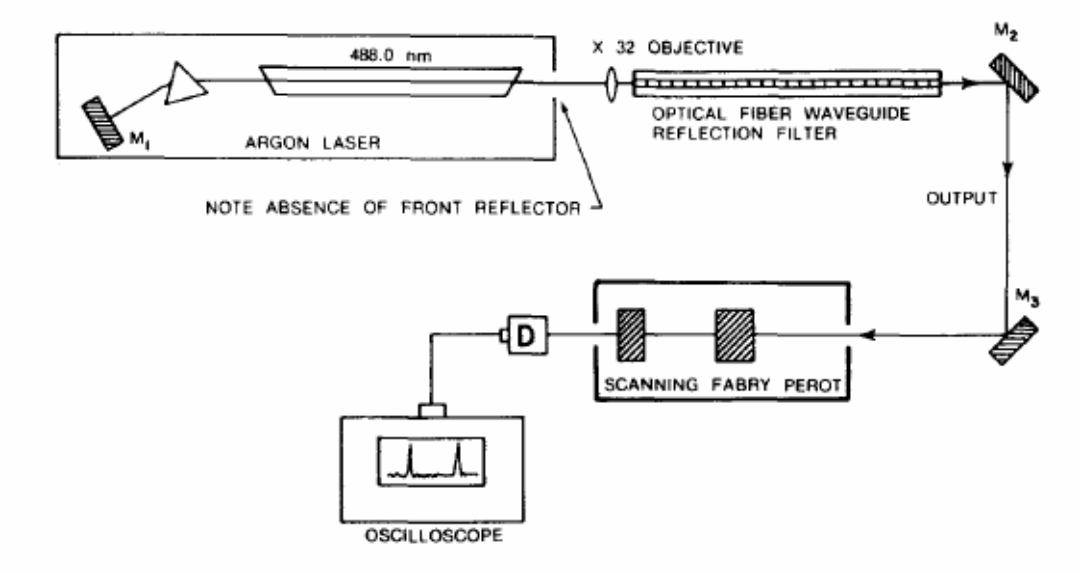

Figure 2.10: The Internal Writing Technique Setup[1]

The internal writing technique has the advantage of being very simple and requires very few optical components. Although the setup is simple there are a few disadvantages. First of all, the Bragg wavelength of the fiber is determined by the wavelength of the laser source and secondly this method only induces a small index change in the fiber which leads to the grating having to be on the order of tens of centimeters [15].

2.4.2 Point-By-Point Technique

Malo *et al.* [33] first demonstrated the method of writing fiber Bragg gratings by writing the index perturbations one at a time along the z-axis of the photosensitive fiber. This fabrication process is known as the point-by-point technique. A single pulse of 248-nm UV light passes through a slit of width (W), which is typically $\Lambda_g / 2$, and a lens is used to image the slit onto the core of the photosensitive fiber which causes an index change in the fiber. A translation stage is used to move the fiber in the z-direction, a distance of Λ_g, so that the next grating plane can be written. By repeating this translation and point writing process a grating is eventually written within the fiber core. A schematic for the point-by-point fabrication setup is shown in Figure 2.11.

By controlling the fabrication of the FBG, point-by-point, the distance between the index perturbations can be changed to fit any imaginable profile. Any sort of novel grating can be created. One such FBG is a chirped grating with a monotonically varying Bragg period over the length of the fiber. Other devices that can be created are spatial mode converters and polarization mode filters [33].

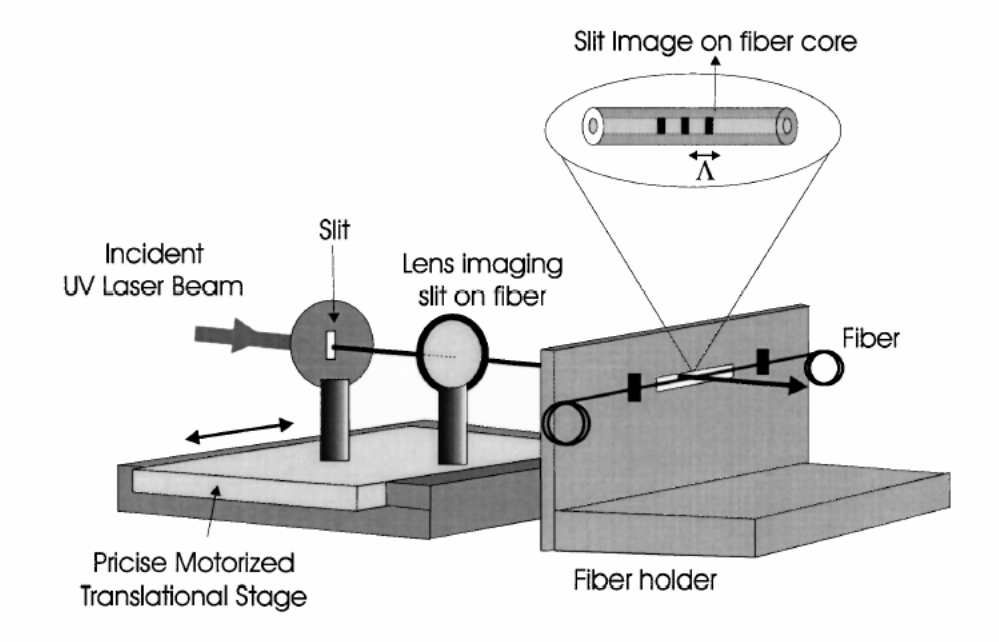

Figure 2.11: Schematic of the Point-by-point fabrication setup consisting of slit, focusing lens, and translation state and fiber holder[28].

The major disadvantage of this fabrication technique is that the process is very time consuming. Additionally, the process is susceptible to variations in strain due to translation stage jitter and/or thermal expansion [15].

2.4.3 Interferometric Technique

Meltz *et al*. [24] used a holographic interferometer to inscribe fiber Bragg gratings into photosensitive fiber, see Figure 2.12. The index modulation in the FBG is created by exposing the fiber to a two-beam interference pattern. The first experiments carried out using the holographic method used a tunable Excimer-pumped argon laser to supply light at 488-nm and a frequency doubling crystal to halve the wavelength to 244-nm, thus providing UV light. By changing the half angle (φ) between the two UV writing beams the Bragg wavelength (λ_B) was modified. The relationship between φ and λ_B is given by

$$\lambda_B = \frac{n_{eff}\lambda_{UV}}{\sin\varphi} \tag{2-12}$$

where n_{eff} is the effective background index of refraction of the fiber and λ_{UV} is the wavelength of the UV laser light[28]. If the angle is kept constant the Bragg wavelength can also be changed by tuning the wavelength of the UV source [34].

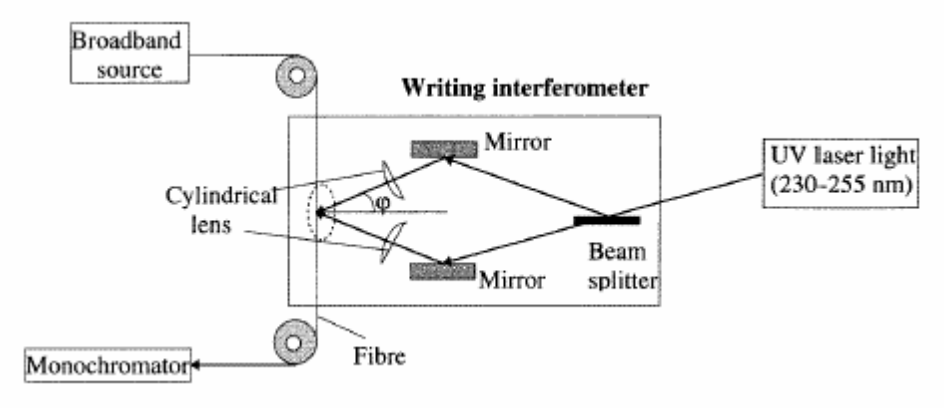

Figure 2.12: Schematic of the two beam interferometer fabrication technique [34]

2.4.4 Phase Mask Technique

The phase mask technique, first developed by Hill *et al* in 1993 [35], is one of the simplest and most effective fabrication methods for FBGs in photosensitive fiber. A phase mask is a device made out of a UV transparent material, in this case silica glass, which has a periodic grating etched into the surface of the device. When UV light is sent through the phase mask at normal incidence an interference pattern is created consisting of the plus and minus first diffraction order. The zero-order is suppressed. When a piece of photosensitive fiber is held in close proximity to the phase mask the interference pattern induces a periodic change in the index of refraction of the fiber, see Figure 2.13.

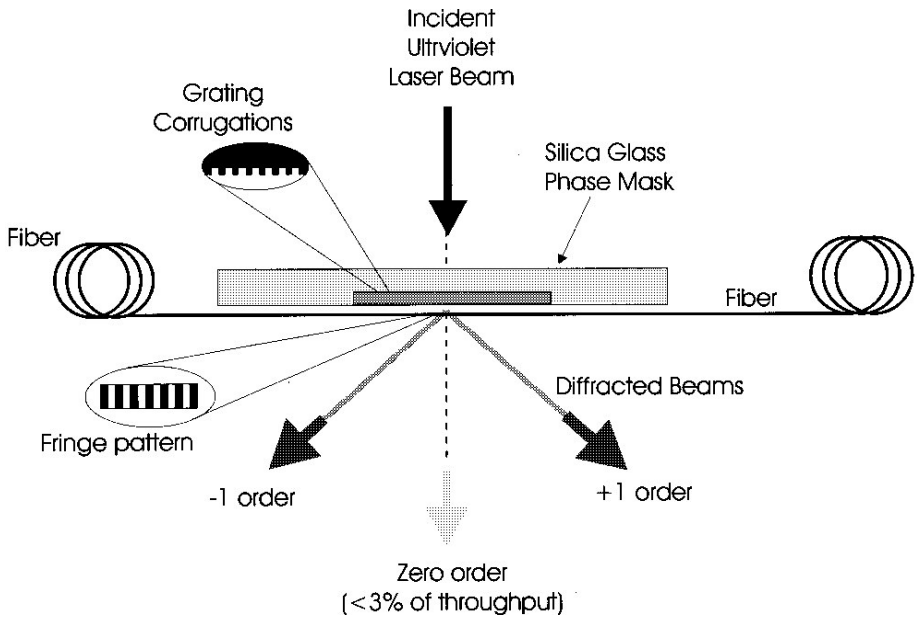

Figure 2.13: Phase Mask Fabrication Technique Schematic [28]

The desired Bragg wavelength (λ_B) is determined by the period of the grating (Λ_{pm}) etched into the phase mask[28], given by

$$\Lambda_g = \frac{\lambda_B}{2n_{eff}} = \frac{\Lambda_{pm}}{2} \tag{2-13}$$

From Equation (2-13) it can be seen that the period of the grating on the phase mask is twice that of the period of the index modulation of the fiber Bragg grating.

The phase mask fabrication technique is widely used due to the fact that the setup is relatively simple. Since the setup is simple and uses only a few components errors induced by vibration are limited. Another benefit of this technique is that the wavelength of the FBG is determined by the periodicity of the phase mask and is not dependent on the wavelength of the incident UV laser light. All of these benefits are ideal for industry due the simple setup and fabrication repeatability [34].

3.0 FIBER BRAGG GRATING FABRICATION

This chapter describes the experimental setup and characterization techniques for fiber Bragg grating fabrication, which utilize the phase mask fabrication technique to manufacture the gratings. The writing setup consists of a 248-nm UV Excimer laser, deep ultraviolet optical delivery system, phase mask, optical fiber alignment stages, and CCD camera visual monitoring system. Using this system, a number of different types of gratings have been successfully written in both hydrogen-loaded standard telecommunication fiber (Corning SMF-28), and 8% Ge-doped photosensitive fiber (Newfurd GF4A). The types of grating written with this setup include uniform Bragg gratings in the S, C, and L-bands, apodised gratings, blazed gratings, linear chirped gratings, long-period gratings, and grating arrays. In the following sections, the optical setup, fiber to phase mask alignment procedure, *in-situ* monitoring techniques for grating inscription, and typical spectra responses of gratings inscribed using this system will be discussed in detail.

3.1 UV EXCIMER LASER AND OPTICAL SETUP

The UV-Excimer laser used in the laboratory was the PulseMaster PM-800 manufactured by GSI Lumonics. The laser operates using a mixture of high pressure gases and is capable of emitting light at the following wavelengths: 193, 248, 308, and 351 nm[36]. A detailed description of the operating principles for the UV Excimer laser can be found in the GSI Lumonics operations manual[36]. The gas mixture and optical setup for the FBG manufacturing system was chosen

so that 248-nm UV light could be used to write FBGs in germanium-silica fibers and hydrogen loaded fibers. The gas mixture for 248-nm emission was a mixture of three gasses. Krypton and Fluorine composed 2% and 0.1% of the total gas, respectively. The rest of the laser vessel was filled with Neon gas to bring the pressure of the vessel up to 5000 mbar[36]. Nitrogen gas was used to open and close the shutter at the output of the laser. The author was responsible for the laser setup and maintenance. The operating characteristics of the laser used for the FBG inscription are summarized in Table 3.1. The detailed operation procedure of the laser can be found in the GSI Lumonics operations manual [36].

Table 3.1: KrF laser parameters for FBG fabrication

Laser Parameter	Value
Wavelength	248 nm
Pulse Duration	~15 ns (FWHM)
Pulse Energy	50 mJ to 850 mJ
Beam area	0.02 cm^2
Pulse Repetition rate	1-100 Hz

The optical setup closely follows the phase mask fabrication setup described in Section 2.4.4, with only a few minor alterations (see Figure 3.1). Figure 3.1(a), not drawn to scale, shows the schematic of the FBG fabrication setup. Figure 3.1(b) is the actual fabrication setup in the laboratory. The minor modification to the setup was the addition of a telescope which made the laser light leaving the telescope more uniform in comparison to the light leaving the output of the laser.

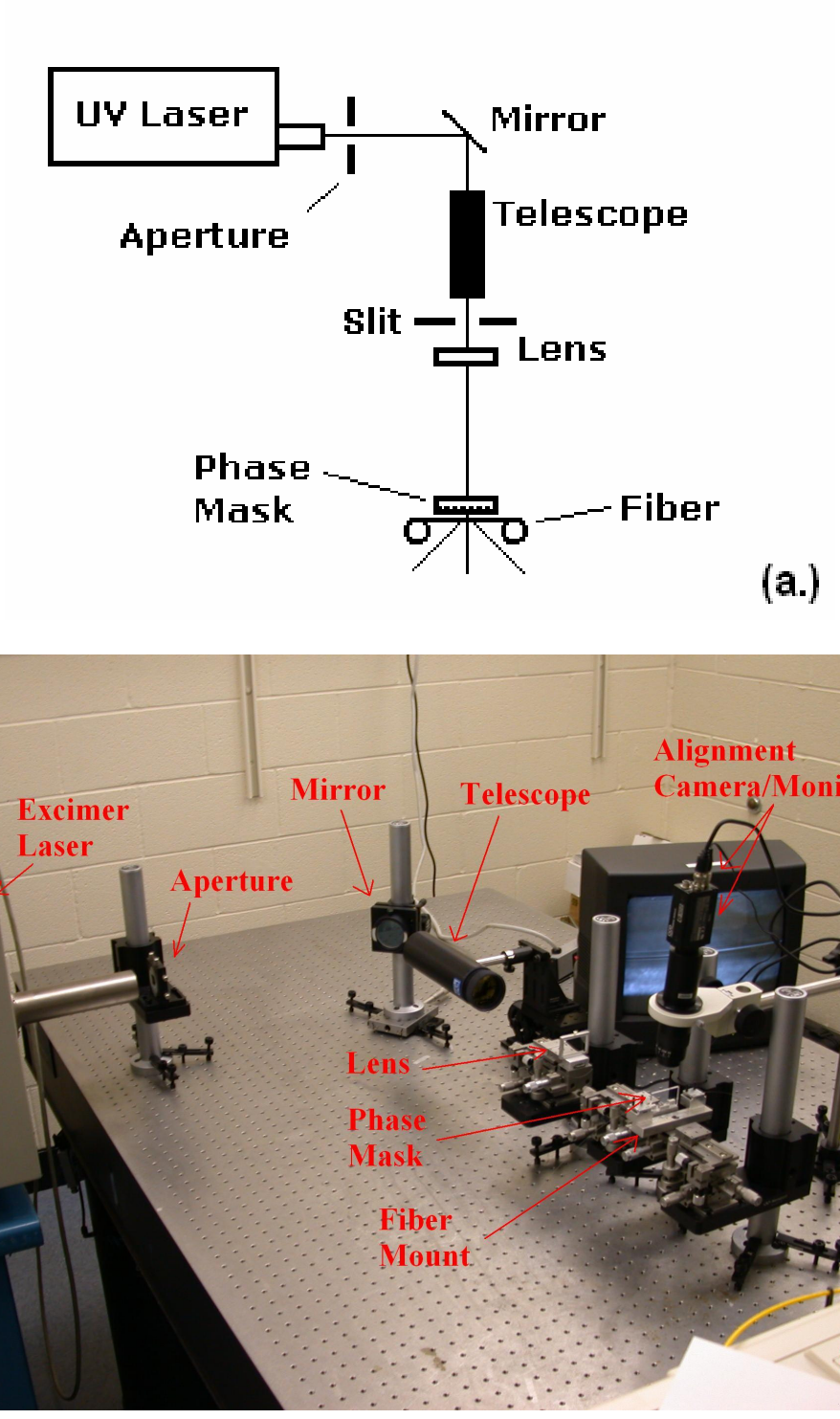

Figure 3.1: (a) Schematic representation of the laser optics for the fabrication setup based on the phase-mask fabrication technique. (b) The actual optical setup for the fabrication system.

A 1-cm by 1-cm rectangular aperture was placed in front of the output of the laser to shape the central portion of the laser beam to the size of the input lens on the telescope. The slit was added before the cylindrical lens to adjust the length of the FBG that was to be written. The cylindrical lens was used to line-focused the output of the telescope. The focal line was set two to three millimeters in front of the phase mask. The light must not be focused onto the phase mask or the fiber that lays a few hundreds of microns in front of the mask, so as to avoid damage to the phase mask. The only role of the mirror was to bend the light, so that the optical bench, where the optics sit, can fit in the space constrained lab.

The on-fiber energy of the laser beam was measured after the cylindrical lens with a pyroelectric detector and power meter (Scientech 361). The fluence of the laser beam was determined by etching PMMA. During the writing process a PMMA sample was exposed to the KrF laser radiation at the position where the fiber was normally placed. The dimensions of the trench created in the PMMA sample were measured using a measuring microscope (Olympus STM-UM). Fluences were determined by the ratio of on-fiber energy to the area of the laser etched trench.

3.2 FIBER ALIGNMENT AND FIBER GRATING WRITING PROCEDURE

The reflectivity of a Bragg grating written by the phase mask technique can be altered by changing any number of parameters, such as the distance the fiber is from the phase mask, the writing time, and the fluence. A series of writing experiments have been carried out using 8% Germanium doped silica single mode fiber ($9\,\mu m/125\,\mu m$) and have results similar to those of Barber and Rizvi[37]. These experiments were carried out in order to ensure that the fabrication setup was properly aligned and comparable to other fabrication setups.

The writing procedure begins with careful preparation of the fiber itself. The polymer jacket of a 6-cm section of test fiber was first stripped and cleaned with methyl alcohol. The end facets of the test fiber were cleaved (Fitel #321) and cleaned to ensure the end facet of the fiber was clean and particle free. One cleaved end of test fiber was then fusion sliced with the output port of a 3-port fiber circulator. The input port and the reflection port of the circulator are connected to a broadband source and an optical spectrum analyzer (Ando 6317C) for *in-situ* monitoring. Alternately, by monitoring the transmission spectrum of the FBG one can eliminate the need for the circulator by directly tying a broadband source and optical spectrum analyzer (OSA) together via the fiber in question. The stripped section of the fiber is then fixed with magnetic strips on a 6-axis mechanical translation stage. Using a CCD camera the fiber was carefully brought close to the phase mask until the gap between the fiber and the reflection image of the fiber was within a fiber diameter of 125 μm (Figure 3.2(a)). Due to the short spatial coherence length of the excimer laser radiation, it is important to maintaining the close proximity between the phase mask and the fiber is essential. However, extra care must be taken to ensure that the fiber does not touch the phase mask in order to avoid contamination.

After the initial alignment, the excimer laser was turned on at low energy (<100 mJ/pulse) during manual alignment. Manual alignment is achieved by adjusting the 6-stage translation stage that houses the fiber. A diffractive pattern of the UV laser beam, after the phase mask and the fiber, can be visualized from a fluorescent pattern when the UV light is projected onto a paper screen (Figure 3.2(b)). The diffraction patterns from the phase mask consist of a number of bright horizontal bars. The fiber appears as the dark shadow inside the brightest diffraction pattern shown in Figure 3.2(b). Fine adjustment is needed to bring the fiber shadow to the middle of the horizontal diffraction pattern.

Once the desired alignment is achieved the spectral response of the FBG should be monitored to ensure that a grating is being written. Monitoring the transmittance of a FBG is the easiest and most cost efficient way in which to measure the spectral characterizations of the grating, since there is no need for a costly circulator, see the measurement setup in Figure 3.3. The transmission spectra of the FBGs were monitored *in-situ* during laser irradiation by a broadband light source (Thorlab ASE7001) and an optical spectrum analyzer (Ando 6317B).

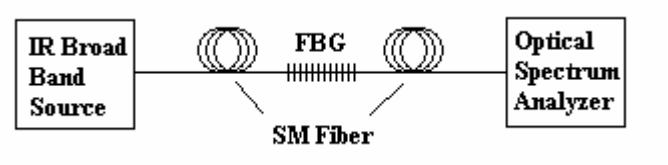

Figure 3.2: Setup for measuring grating Transmittance in 8% germanium doped silica fiber.

In these experiments the transmittance was plotted as a function of the writing time (Figure 3.4). The transmittance was then converted into reflectivity using the following relationship:

$$R = 1 - 2^{-(T/3.11)} \tag{3-1}$$

where T is the absolute value of the peak transmittance minus the transmittance of the broadband source, which was -25 dB. The reflectance was then converted to the index modulation (Δn) using Equation (2-7), so that the change in the index could be plotted as a function of the total exposure dose, see Figure 3.5.

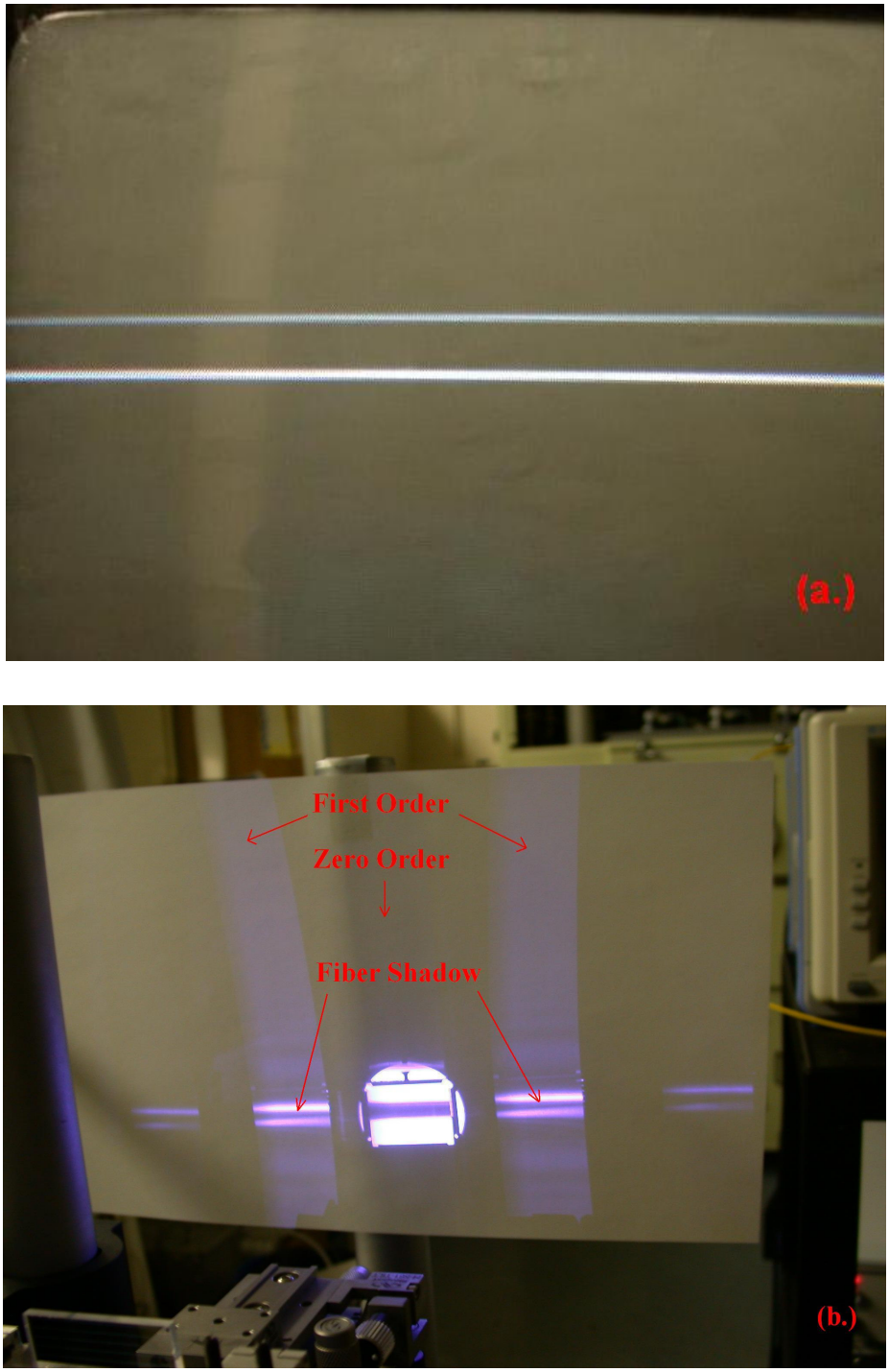

Figure 3.3: (a) The mirror image of the fiber against the phase mask for use in manual alignment. (b) The fringe pattern caused by the grating onto the fiber with zero order suppression, note the shadows created by the stripped fiber.

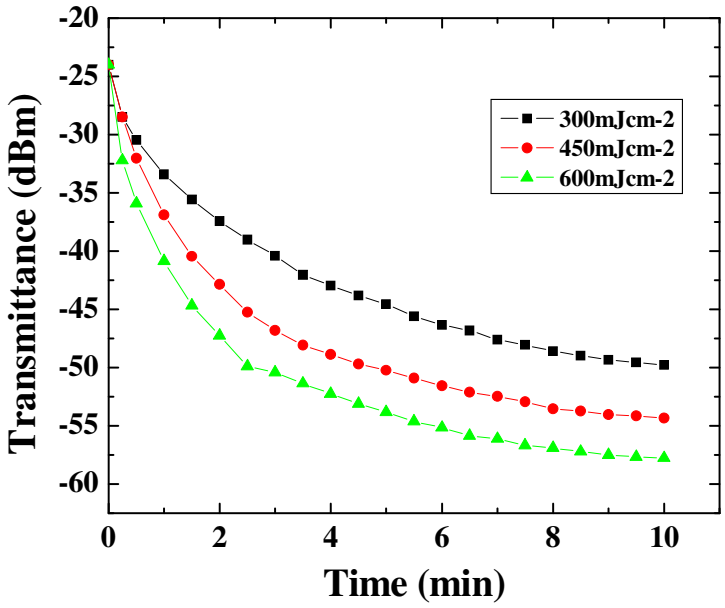

Figure 3.4: Transmittance vs. exposure time for 8% germanium doped silica fiber at three different fluences.

The plot of the transmittance verse writing time is shown in Figure 3.4. The experiment was carried out on 8% Ge-doped photosensitive fiber. Three fluences were used to fabricate the FBGs at 300 mJ/cm^2, 450 mJ/cm^2, and 600 mJ/cm^3, respectively. A uniform 4-cm grating with a transmittance of -55 dB can be readily inscribed in the fiber within 10 minutes at a laser repetition rate of 35 pulse/second. A 35-dB uniform grating of 4-cm length can be fabricated within 30 seconds using 600 mJ/cm^2 and a repletion rate of 35 pulse/second. There is no sign of fiber degradation at any of these fluences. The results are also consistent with the results reported by Barber and Rizvi[37].

In Figure 3.5 the same data presented in the previous figure is presented as the total index change of the grating as a function of the total exposure dose. Comparing the results, Barber and

Rizvi needed an exposure dose of 9000 J/cm^2, much higher than the author's dose of 600 J/cm^2 to achieve a grating strength of -26 dB[37].

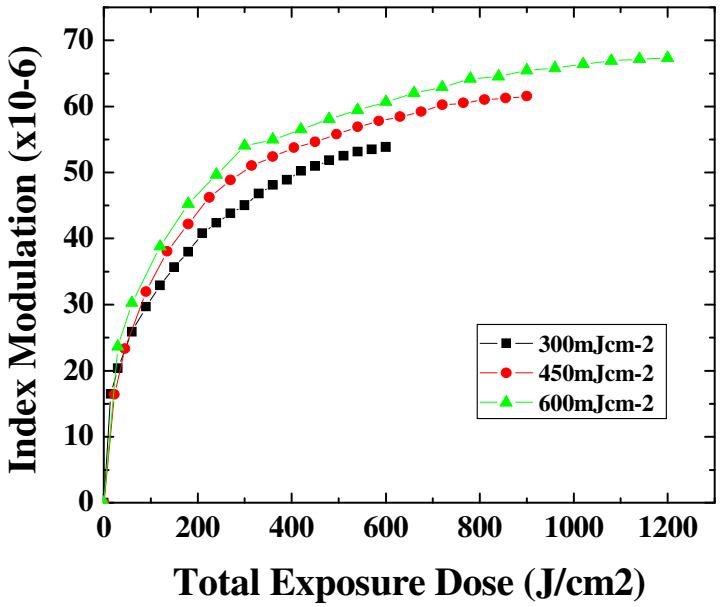

Figure 3.5: Index modulation vs. Total exposure dose for 8% germanium doped silica fiber at three different fluences.

Figure 3.6 shows the final transmission spectra of each of the three FBGs written at different fluences. As the total energy increases, the center wavelength of the transmission valley should increase, however this is not the case for the grating written at the highest fluence. One possible reason behind the unexpected wavelength could be due to a possible misalignment, since each time a new grating is written the position is set manually. The data in Figure 3.6 brings to light the effects of misalignment even though the growth evolution was not affected, as shown in Figures 3.4 and 3.5. Overall, the alignment of the laboratory fabrication system is adequate if not better than other similar systems[37].

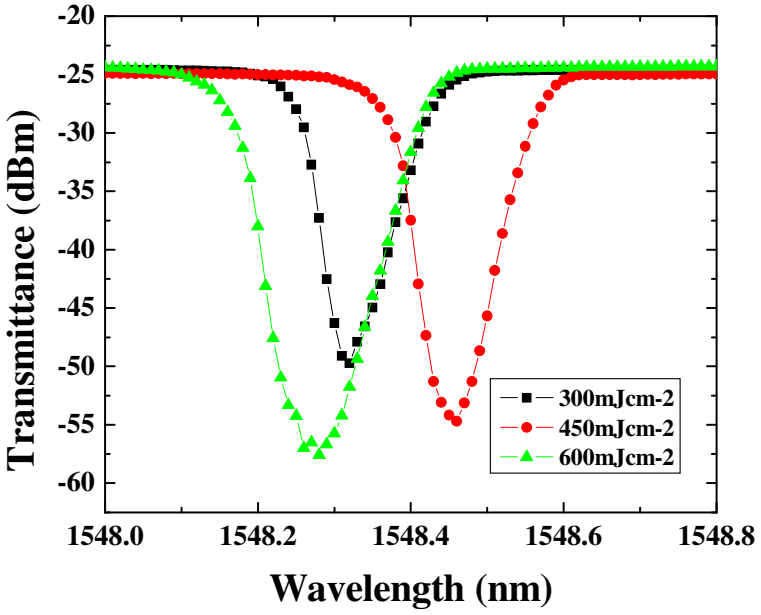

Figure 3.6: Final spectral response of gratings written into 8% germanium doped silica fiber at three different fluences after a period of ten minutes.

3.3 GRATING FABRICATION

The in-house fabrication system is also capable of fabricating many other types of fiber Bragg gratings, such as common Bragg grating arrays, blazed gratings, and chirped gratings. By manipulating the optics (i.e. changing the phase mask, fiber alignment, or slit width) these different gratings can be written at various wavelengths and/or strengths. In this section a common Bragg grating array will be discussed.

3.3.1 Common Bragg Grating Fabrication

The common Bragg grating is the simplest grating to write with our in-house fabrication system. By utilizing the setup in Figure 3.1 and keeping the fiber completely parallel to the grating the common Bragg grating was written. The spectral response of a common Bragg grating was shown in Figure 2.6.

By putting multiple gratings on a single fiber an array is created which can be used in multipoint sensing and communications. One application is the use of a FBG array for multipoint strain sensing for smart structures, such as load monitoring in a bridge[9].

There are at least two different ways to write an array of fiber Bragg gratings on a single piece of fiber utilizing the phase mask fabrication technique. The first method is to use a different phase mask with a different grating period for each FBG in the array. This method can be tedious and time consuming due to the fact that the fabrication process must be interrupted so that a new phase mask can be inserted behind the fiber. A more efficient method of writing gratings at different Bragg wavelengths along the z-axis of the fiber is by applying a strain to the fiber as UV light induces the periodic index change. First demonstrated by Zhang *et al*. an applied axial strain of 0.2% resulted in a wavelength shift of 2.5 nm[38]. There are limits to the tuning method since the fiber can only withstand a strain of no more than 5%[15].

The fringe pattern caused by the UV light hitting the phase mask has a constant period and once the strain is removed from the fiber the spacing between the index changes, which causes the Bragg wavelength of the grating to decrease. Therefore, by controlling the applied strain, multiple gratings with different Bragg wavelengths can be written into the same fiber using only one phase mask.

In Figure 3.7 the reflectivity of a four grating array is shown where the spacing between each grating is on the order of 1 nm to 1.5 nm. The gratings were written into a piece of single mode 8% germanium doped silica fiber with a grating length of 5 mm. Due to the fact that the strain applied to the fiber during the writing process was done manually there is no way to accurately space the gratings. By automating the writing process precision grating spacing can be achieved.

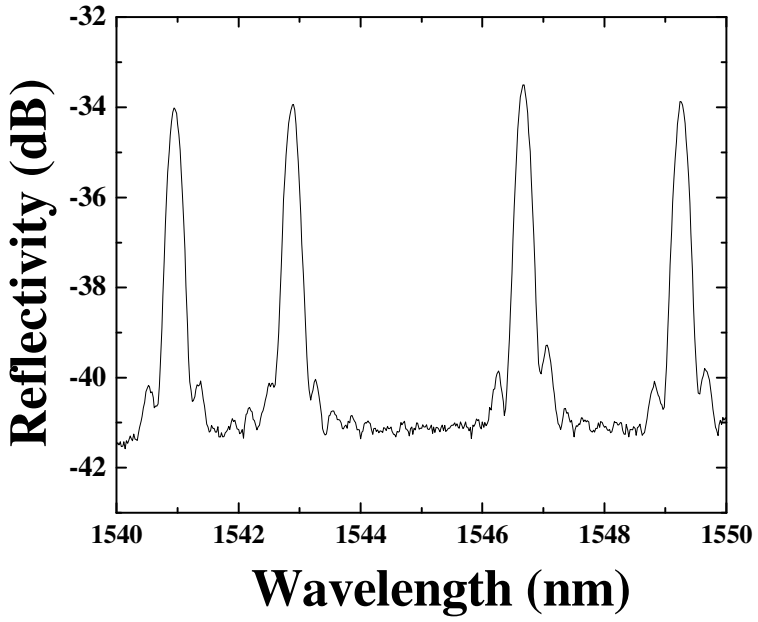

Figure 3.7: Reflectivity of a four 5-mm grating array on a single piece of 8% Ge-doped silica fiber.

4.0 TUNABLE FIBER BRAGG GRATINGS

Tunable fiber optical components such as tunable fiber Bragg gratings are key components in optical communications and for fiber sensing. Fiber Bragg gratings exhibit tunability when an external perturbation is applied to the grating, which modifies the spectral response. In Section 2.2.2, the sensitivity of the grating to either temperature or strain was discussed and the majority of tuning mechanisms are based on one or both of these external perturbations. Tuning mechanisms include on-fiber electrical heating [3, 8, 17-19], bending and stretching due to the piezoelectric effect [7, 20], mechanical bending and stretching [21, 22], and acoustic modulation [5]. Tunable gratings are useful in wavelength demultiplexing systems, as tunable filters, and for active sensing. In the subsequent sections various tuning mechanisms will be discussed and the in-fiber laser light tuning mechanism, developed by Dr. Kevin P. Chen and associates, will be presented.

4.1 TUNING METHODS FOR FIBER BRAGG GRATINGS

Several novel approaches to tuning FBGs exist, some of which are more practical than others. Most tuning mechanisms use electricity and/or mechanical means of tuning. Some of the more common electrical tuning methods are heating by applying electrical energy to resistive thin films[8] or using Peltier heating elements[18]. One electro/mechanical method involves a strain being applied to the fiber grating as voltage is applied to a piezoelectric material [7]. A purely mechanical method, created by Goh *et al*., involves a FBG embedded into an elastic substrate in

which a knob controls the amount of strain by compressing the substrate[22]. These various tuning methods will be discussed as a basis for comparison for the tuning method using in-fiber laser light.

4.1.1 Mechanical Tuning by Beam Bending

The beam bending method of tuning which utilizes a structure that applies a force via a micro adjust knob onto a flexible substrate, has a tuning range of about 90nm (Figure 4.1). The device can be used in applications such as tunable fiber lasers, dynamic add-drop demultiplexers, and narrow-band tunable filters[22]. Although the tuning range from 1634 nm to 1544 nm is one of the largest tuning ranges ever reported for a fiber Bragg grating, the beam bending structure is also by far one of the most cumbersome tuning methods. Another drawback to the system is that the tuning mechanism is a manual system and in order to make the system more automatic, an addition of another system, such as an electric motor, would have to be included, further adding to the bulk and cost.

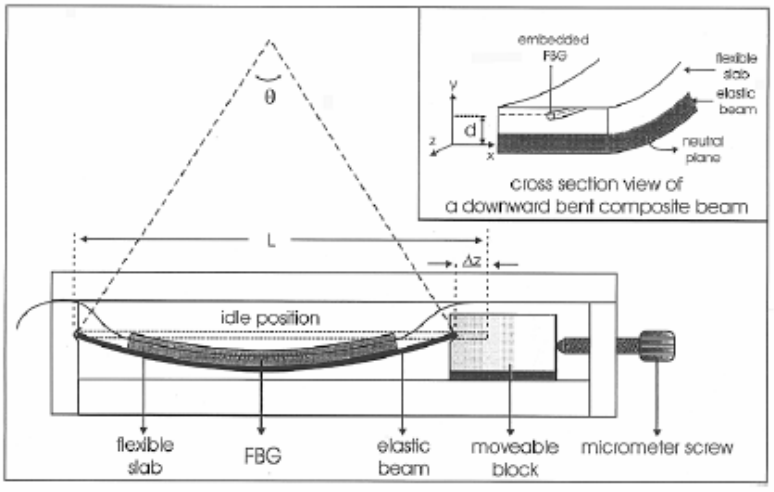

Figure 4.1: Mechanical beam bending tuning method setup with a tuning range from 1634 nm to 1544 nm[22]

4.1.2 Electro-Mechanical Tuning by PZT substrate

The electro/mechanical tuning method uses a piezoelectric substrate to apply a strain to a non-linearly chirped grating (see Figure 4.2). This particular grating and tuning mechanism was to be used for dispersion compensation. The PZT substrate and the electrical contacts between the high voltage source and substrate add a considerable amount of bulk to the FBG. Comparing the PZT tuning method to that of the solely mechanical system presented by Goh *et al.* there is a significant improvement in having the bending controlled by an applied voltage rather than by mechanical means.

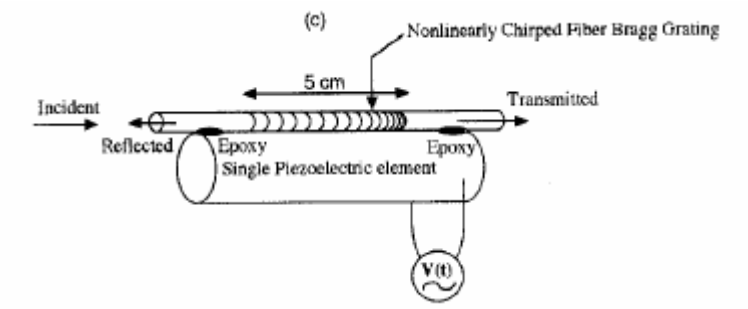

Figure 4.2: The PZT tuning mechanism[7]

4.1.3 Tuning by Electrically Powered Resistive Coating

A solely electrical tuning method involves the use of a resistive coating applied to the outside of the FBG, on the order of a few microns thick. Electrical leads are attached to the resistive coating and when electrical energy is applied the thin film heats up which causes the Bragg wavelength response of the coated grating to shift. The shift in the response of the grating occurs by a combination of thermal induced index change and thermal induced expansion, as demonstrated by Equation (2-11).

Limberger *et al.* created an electrically tuned reflection filter by coating a grating with a 20-nm layer of Titanium followed by another 300-nm layer of Platinum by dc sputtering, where both layers were uniform[3], see Figure 4.3(a). The titanium was used as a bonding agent between the platinum and the silica fiber. By attaching gold leads to the platinum a complete resistive heater was created and by applying electrical current to the heater a 2.15-nm resonance shift was observed with a slope of 4.1-nm per watt. Given the small Bragg wavelength shift observed it can be said that at higher current either the resistive coating or electrical leads broke down and that by making the coating thicker a larger shift could be observed. A possible drawback to increasing the thermal mass of the resistive coating is that the response time of the device will increase.

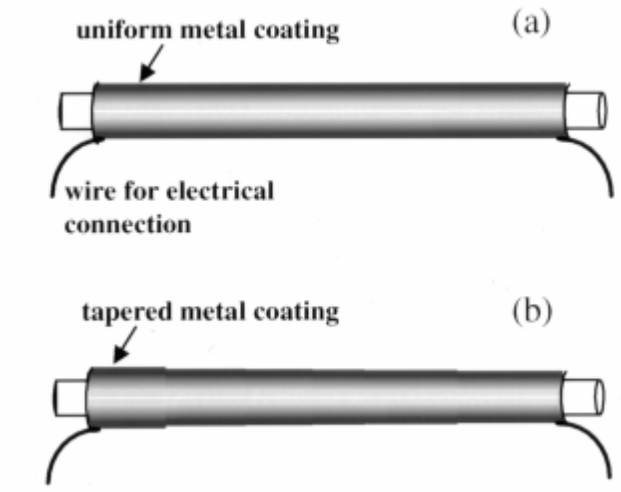

Figure 4.3: (a) uniform metal coated resistive heater. (b) Tapered metal coated resistive heater.

By changing the composition of the resistive coating, such as gradually increasing the thickness along the z-axis, a chirped grating can be created from a uniform Bragg grating. Rogers *et al*. created a tunable chirped Bragg grating by coating a fiber with a distributed on-

fiber resistive coating[8], see Figure 4.3(b). As current passes through the tapered coating, more heat is generated at the thinner portion, so that a temperature gradient is created, causing a gradual change in the index of refraction along the z-axis, which creates chirp. The coating is created by a complex process where 10-nm of titanium is applied, followed by 150-nm of gold, to create a uniform coating on the fiber. Once this is done a translation stage is used to pull the fiber from an electroplating bath of silver so that a gradual variation in the thickness of the metal is electroplated onto the gold layer, the minimum thickness of the electroplating is 5 μm with a maximum thickness of 20 μm. With an applied voltage of 1.1 volts the chirp increased from 0.4 nm to 1.2 nm. The important ramification of this type of coating is that by changing the thickness profile many different chirp profiles can be created.

4.2 TUNING FBGS BY IN-FIBER LIGHT

A method of tuning without the use of wires, where the control signals and power is delivered optically and is self contained within the same fiber, is the tuning method using in-fiber laser light[16]. The method developed by Chen *et al*. has the same benefits as that of the tapered resistive coating method, such as having the ability to create chirping profiles in a uniform Bragg grating, but there is no longer a need for electrical wiring and contacts. Also by using short Bragg gratings, chirped gratings are not created and the reflectance peak of the grating is not distorted. The tuning is done completely by optical means and the benefits of optical fiber components such as long lifetime, immunity to electromagnetic fields, low cost, and the capability to function in harsh environments, due to failure of electrical contacts and wiring, is not lost. Another benefit of tuning by in-fiber diode laser light is the ability of the devices to be

easily embedded for use in smart structures since bulky tuning methods are no longer attached to the device. This section presents tunable fiber Bragg gratings without the need for sophisticated packaging and external electrical connections. The resonance wavelength, spectrum width, and chirping of FBGs can be directly controlled by in-fiber light.

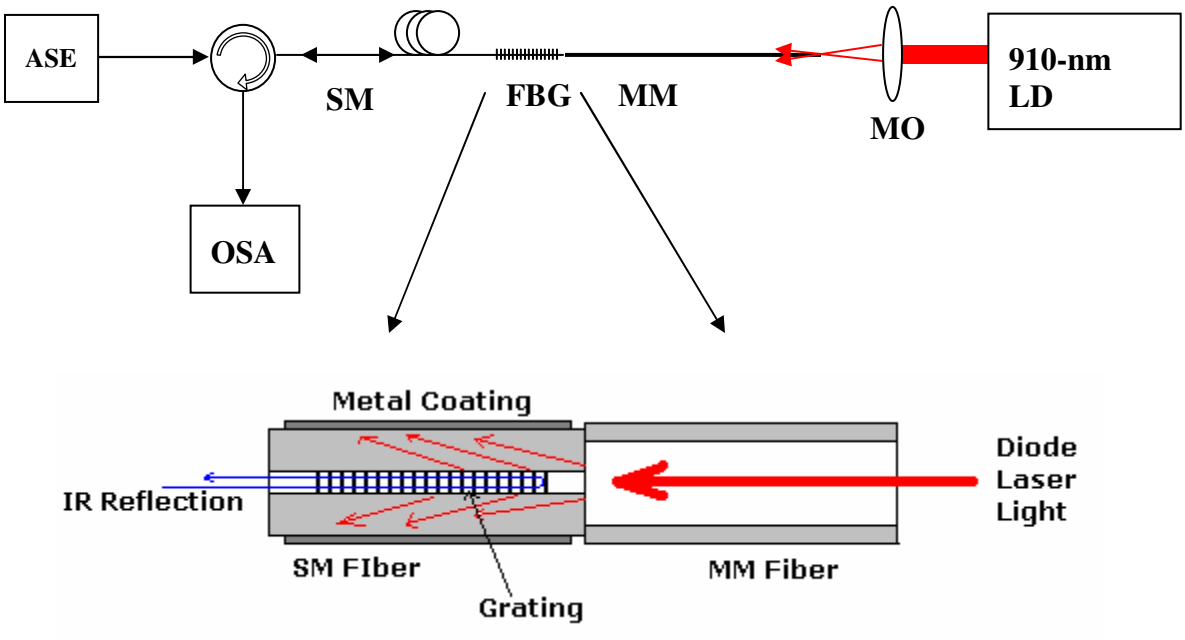

Figure 4.4: Prototype of a fiber Bragg grating (FBG) sensor in a single-mode (SM) fiber powered by light. Light from a high-power laser diode (LD) was focused by a pair of 20× microscope objective (MO) and coupled into a multimode (MM) fiber, which is fusion spliced to the SM fiber. Due to the mode mismatch between the two fibers the leaking light is absorbed by the metallic coating and the FBG is heated.

The tunable FBG presented here involves two sections of fiber as shown in Figure 4.4. A FBG was written in a single-mode standard fiber (Corning SMF-28). The reflection spectra of the FBG were monitored with an optical spectrum analyzer (Ando 6317C) and a broadband source, via a circulator. The single-mode fiber was fusion spliced with a 100-μm core multimode fiber (140-μm diameter, N.A. 0.22). A uniform silver film was plated on the FBG section of the fiber with a resistivity of 2.2 Ω /cm. The coated section was approximately 5-mm

from the spliced junction. The thermal expansion coefficient for silver is 5.5×10^{-6}/K in contrast to 0.66×10^{-6}/K for silica glass. Uniform gratings with lengths of 4-mm and 4-cm, as well as, a 4-cm linear chirped grating were used in the experiments.

Ten watts of 910-nm laser light from a high-power diode laser array was coupled into the end of the multimode fiber using a pair of 20× microscope objectives. The coupling efficiency was approximately 10%. This low coupling efficiency was probably due to the poor beam quality of the diode laser array. The 910-nm laser light propagating in the multimode fiber leaked into the cladding of the single-mode fiber through the spliced junction, shown in the inlet of Figure 4.4. The leaking light was subsequently absorbed by the metallic coating, which created heat and raised the temperature of the FBG.

By using the cut back method the light loss profile was estimated and followed a monotonically decaying exponential curve with a constant loss coefficient. In Figure 4.5 the normalized light leaving the fiber was plotted as a function of the distance from the junction between the single mode and multimode fiber.

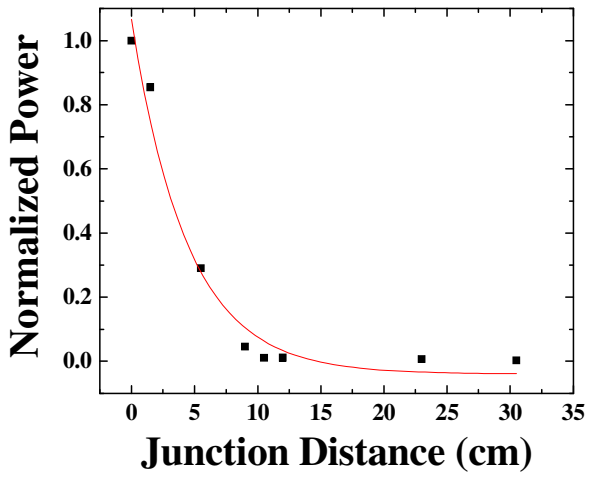

Figure 4.5: Normalized power loss as a function of the distance in centimeters from the SM-MM junction.

At a distance of 20 centimeters from the junction 99% of the laser light was lost. Using a data analysis program the equation for the light loss from the junction was found to be:

$$\frac{P(z)}{P_o} = 1.1e^{-z/4.4} \tag{4.1}$$

Where z was the distance from the SM-MM junction in units of centimeters and P_o is the laser power right at the SM-MM junction. Using this equation approximately 10% and 60% of the diode laser light leaked out from the 4-mm and 4-cm FBG sections, respectively.

4.3 TUNING BY IN-FIBER LIGHT EXPERIMETNAL RESULTS

Figure 4.6 shows the spectrum evolution of a 4-mm uniform FBG heated by 910-nm laser light with a total input power of 1-W. 130-mW of the laser light was estimated to have leaked through the 4-mm section of the fiber containing the grating. Since the thermal mass of the 4-mm FBG was only 200-μg, the absorption of 130-mW of diode laser light raised the temperature dramatically and shifted the resonance wavelength up to 4.9 nm. The eight times larger thermal expansion coefficient of silver film over silica fiber may also play a significant role in the resonant wavelength shift [39]. The optical power was delivered by the same fiber containing the FBG and almost all of the optical energy was used to heat the grating, except for a very small portion of the thermal energy which was wasted on the fiber coating.

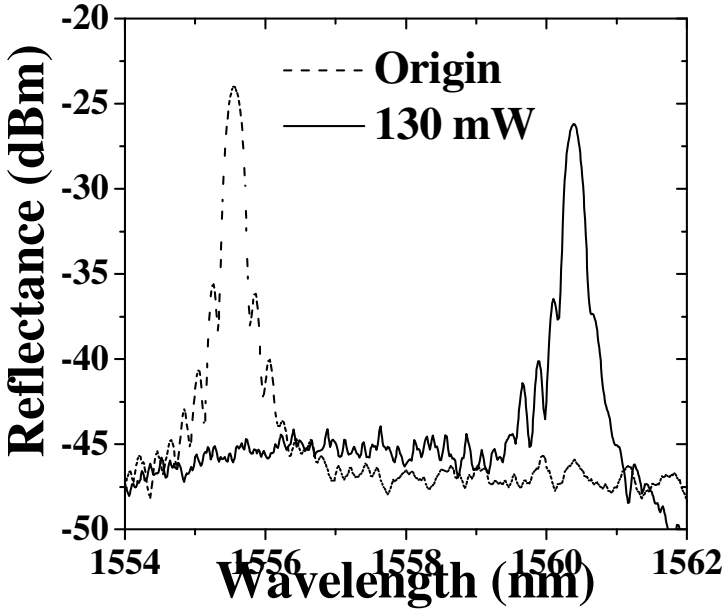

Figure 4.6: Resonance wavelength shift of a 4-mm FBG heated with 130-mW of in-fiber diode laser light at 910 nm.

The resonance wavelength shift as a function of the input laser power is shown in Figure 4.7. The sudden increase of the wavelength shift at the 130-mW input laser power may be attributed to coating degradation on the fiber at the elevated temperature, which leads to an absorption increase and significant change of the thermal expansion coefficient of the metal coating. The settling time and tuning stability of the optically powered FBG was observed at an input laser power of 45-mW while the heated FBG's resonance wavelength shifted 1-nm from the origin. The settling time constant while the optical-powered FBG shifted over a range of 0.73 nm is estimated to be less than 0.5 s, which is similar to FBGs tuned by electric heaters [3]. The heated FBGs are very sensitive to surrounding air flow disturbances. The thermal responses of optical-powered FBGs change dramatically while the heated FBGs are submerged in liquids.

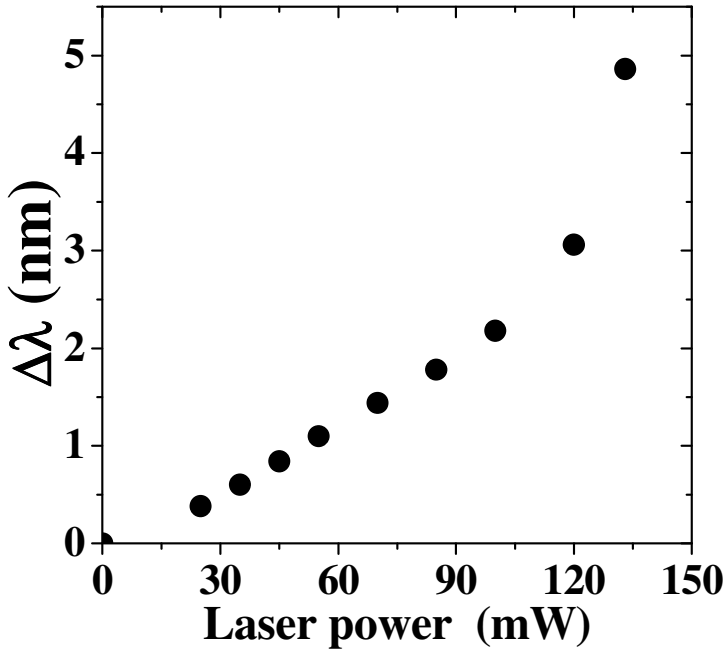

Figure 4.7: The resonance peak shift as a function of the input laser power for a uniform 4-cm grating

The light energy leaking out from the fiber cladding falls off exponentially with distance (assuming a constant loss coefficient), thus a temperature gradient is created in longer FBGs. The temperature gradient modifies the spectral response of FBGs and can be used to control grating chirps. Figure 4.8(a) shows the spectrum stretch of a 4-cm long uniform grating with a 0.4-nm spectrum width. The 250-mW diode laser light raised the grating temperature from the input side and increased the background index, which stretched the width of the FBG spectrum to 6-nm.

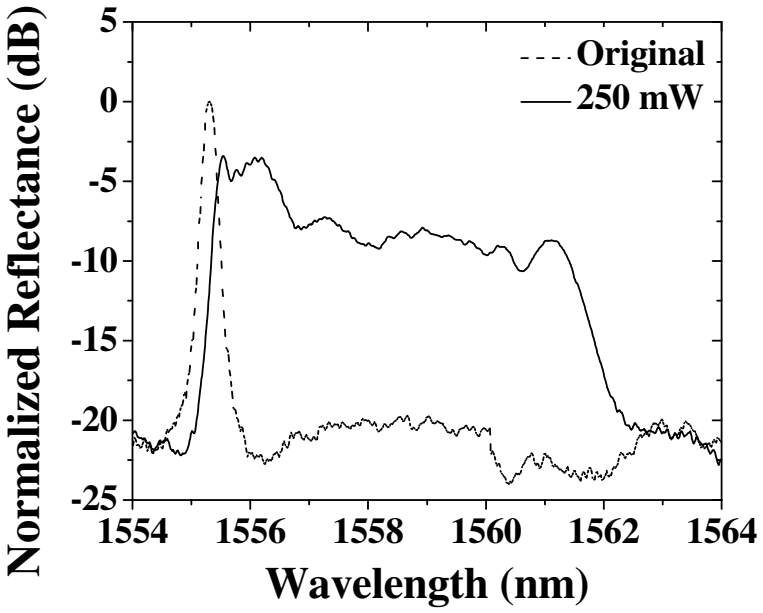

(a)

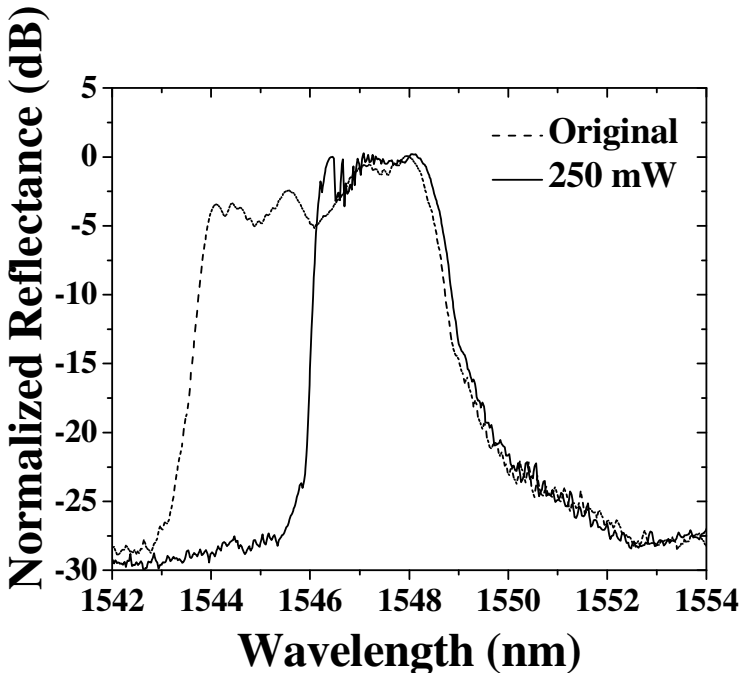

(b)

Figure 4.8: (a) spectrum stretch of a 4-cm uniform grating heated by a 910-nm diode laser with 250-mW of total input light power (120-mW of power was leaked through the grating section). (b) Spectrum compression of a 4-cm linear chirped grating heated by the same input laser power.

Figure 4.9 shows the widening of a spectrum of a 1.7-cm uniform Bragg grating that had undergone chirping due to the temperature gradient caused by the leaking light. An input laser light of eight tenths of a watt resulted in a spectrum widening of 6 nm, for a general widening of 0.75-nm per 0.1 watts of laser power.

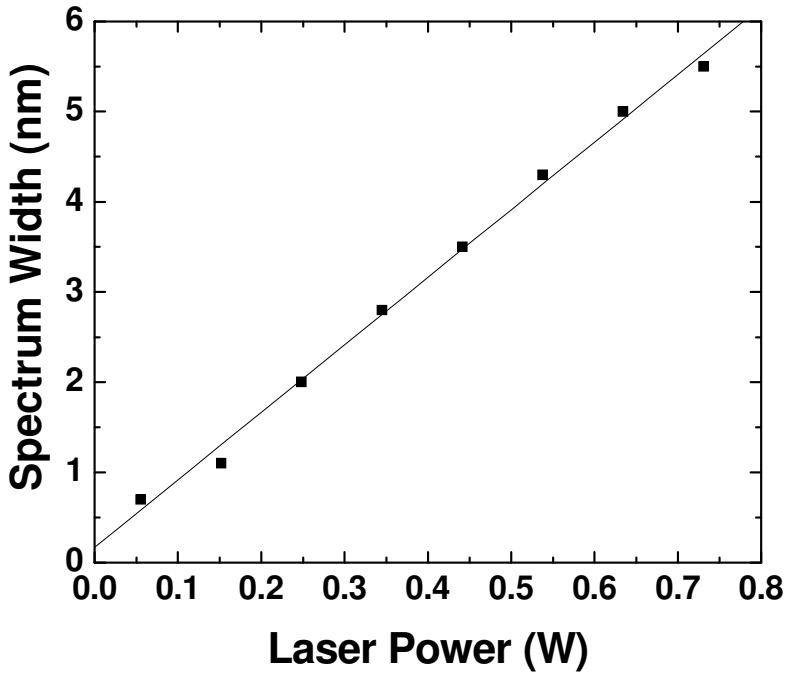

Figure 4.9: Spectral widening of a uniform 1.7-cm Bragg grating sing in-fiber diode laser light. A 6-nm widening occurred with an input laser power of 0.8 Watts.

The reflection spectrum is not flat, suggesting a nonlinear chirp due to a possible exponential temperature gradient in the fiber. By adjusting the coating composition and profiles, it is possible to control the temperature gradient in the uniform FBG to produce chirped gratings with an arbitrary chirping profile. The tuning flexibility of light-powered FBGs can be further demonstrated by a chirped grating spectrum compression shown in Figure 4.8(b). Diode laser light at 250-mW was launched into a 4-cm linear chirped grating (2 nm/cm) from the short

wavelength side. The temperature gradient created by the diode laser light in the FBG "de-chirped" the grating and compressed the width of the grating spectrum from 8-nm to 4-nm.

The appealing advantage of light-powered FBGs is the capability to produce a very small local index change by generating a local light absorber to tailor the reflection spectrum of a chirped FBG. This is demonstrated in Fig. 4.10(a). A 4-cm long linear-chirped FBG (1-nm/cm chirp) with 99% peak reflectivity was first coated with silver film. The coating was subsequently removed by a laser ablation process except for a 2-mm section in the FBG region, which served as a local light absorber. The laser-induced temperature raise changed the local refractive index around the coated section and red-shifted the resonance wavelength of the chirped FBG at the heated zone to the longer wavelength. Due to the reduced grating strength in the heated region a notch filter was produced in the FBG reflection spectrum shown in Fig. 4.10(a). In this experiment a 9-dB notch was producible in the FBG reflection spectrum. The strength of this dynamic notch filter can be controlled by input laser power shown in Figure 4.10(b) by measuring the notch strength as the input laser power was increased.

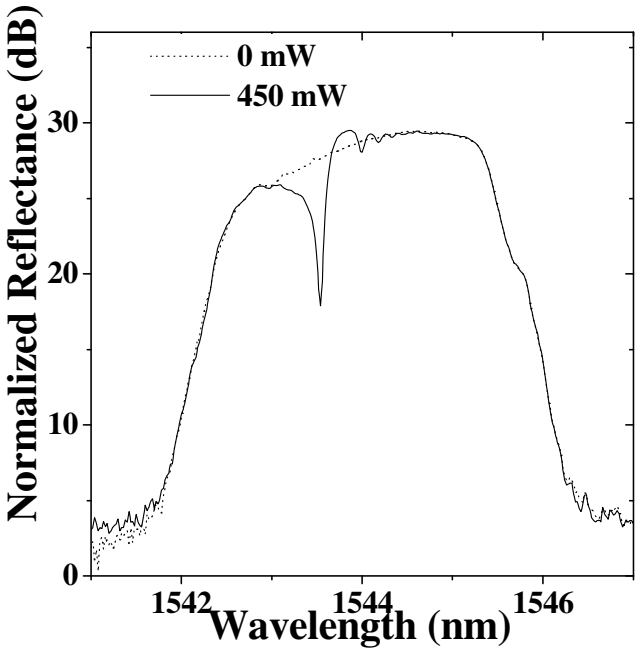

(a)

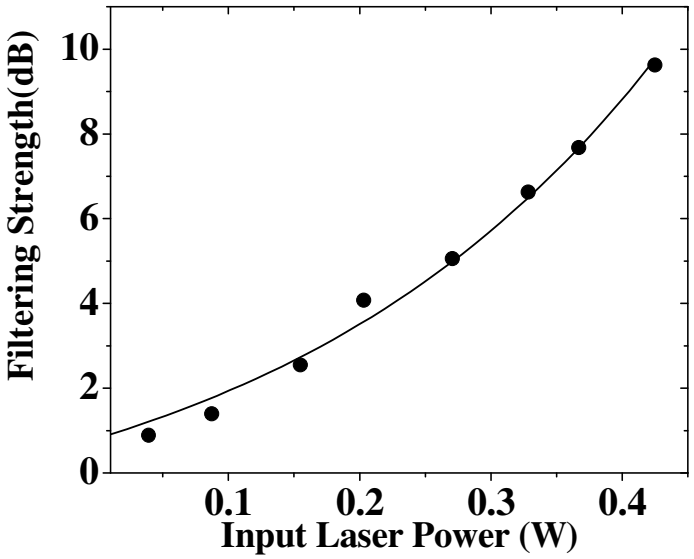

(b)

Figure 4.10: (a) Dynamic fiber notch filter in a linear chirped FBG, a 9-dB notch was induced by 450-mW of input laser power. The Notch filter strength as function of the input diode laser power at 910-nm is shown in (b).

4.4 DISCUSSION

Tunable components powered by in-fiber light offer great tuning flexibility while preserving all the advantages of in-fiber components such as long lifetime, immunity to electromagnetic interference, and the capability of working in harsh environments. The ultimate range of remote tuning using 910-nm laser light is less than 10 km due to a large attenuation (2dB/km) of multimode fibers at this wavelength. The range can be extended by using a longer wavelength pump laser. Fibers are used not only for optical signal delivery, but also as multi-function cables to deliver optical energy and potential control signals. The low-loss cladding of the fiber is ideal for delivering energy for low-power consumption applications (100-300 mW), such as on-fiber micro-heaters and light sensitive polymer membranes. A flow sensor tuned with on-fiber micro-heaters powered by in-fiber light technology will be discussed in the next section.

5.0 LIGHT POWERED TUNABLE FIBER BRAGG GRATING FLOW SENSOR

This chapter presents an active fiber Bragg grating temperature and flow sensor based on self-heated optical hot wire anemometry. The grating sensors are directly powered by optical energy carried by optical fibers. In-fiber diode laser light at 910-nm was leaked out from the fiber and absorbed by the surrounding metallic coating to raise the temperature and change the background refractive index distribution of the gratings. When the diode laser was turned off, the grating was used as a temperature sensor. When the diode laser was turned on, the resonance wavelength and spectral width change of the self-heated grating sensor was used to measure the gas flow velocity. The grating flow sensors have been experimentally evaluated for different grating length and input laser power. The grating flow sensors have demonstrated a minimum measurable flow velocity of 0.35 m/s for nitrogen flow at atmospheric pressure.

5.1 INTRODUCTION

Precise measurement of gas and liquid flow are important for many applications in the chemical, aerospace, and medical equipment industries. Several approaches have been employed for mass flow measurement, which include the following methods: time of flight[40], differential pressure[41], and heat transfer[17, 42-46]. At present, the majority of state of the art miniaturized flow sensors are fabricated using micro- machined- mechanical systems (MEMS) technology on silicon substrates[42-45, 47]. MEMS flow sensors based on both heat transfer and differential pressure measurements have been extensively reported. The flow sensors based on

MEMS technology offer many important advantages such as small size, high sensitivity, and fast response time, but there are a number of disadvantages as well. Although MEMS flow sensors created using silicon micromachining techniques are miniature devices the packaging of these devices are bulky and require at least two metal leads for both the power supply and sensing signal. The bulky packaging and electrical contacts limit the use of MEMS flow sensors from a number of important applications in harsh environments. Such harsh environments may appear in applications in chemical engineering and the aerospace industry, which include fuel injection rate measurement for cryogenic engines and flow measurement in corrosive gas or liquid environments. Also the MEMS flow sensors are not immune to electromagnetic fields and are not practical for flow measurement in confined tubing which is found in medical applications.

Flow measurement has also been reported using optical fiber devices which are based on fiber bending[41, 48]. The principle behind fiber bending is that the device operates by measuring the laser light loss as a flow applies a force to a fiber, misaligning it from the sensing fiber. Compared with electronic and MEMS sensors, fiber optic sensors are ideal for use in harsh environments and applications that have confined space requirements. Optical fiber flow sensors have a number of inherent benefits which include and are not limited to low manufacturing cost, long lifetime, immunity to electromagnetic fields, and high sensitivity. Although these benefits are an improvement over electrical and MEMS devices, limitations still exist on performance and functionality. Certain applications of fiber sensors have been limited by their total passivity. That is their inability to be controlled by external forces for active sensing, such as set point control and tuning, which allow the sensors to adapt and be reconfigured to their surrounding environments.

The research in this thesis presents a new class of multi-functional active optical fiber sensors that are directly powered by in-fiber laser light. Based on self-heated hot-wire anemometry, fiber Bragg grating flow sensors with measurement performance matching or exceeding that of MEMS based flow sensors have been demonstrated. The active fiber sensor is free of electrical components and is directly powered by optical energy. The optical energy is directly delivered to the sensor via the optical fiber rather than through electrical wiring. The sensing signal is detected by an in-fiber Bragg grating and transmitted through the same fiber. The resonance wavelength or chirp of the grating (set-point), triggering time, responsivity, dynamic range, and operational frequency of the flow sensor can be directly controlled though the optical fiber, which allows the sensor to adapt to the surrounding environment for active sensing. The sensing configuration and energy delivery mechanism minimize both electrical and optical cabling, so that packaging and manufacturing costs are reduced. Also by eliminating the use of external connections the sensor can operate in both conducting and non-conducting mediums as well as having the ability to function in confined spaces. In the subsequent sections the design, optical power delivery system, and experimental results of the active FBG flow sensor will be presented.

5.2 SENSOR DESIGN AND EXPERIMENTAL SETUP

Similar to the experimental setup presented in Chapter 4, the FBG flow sensor presented here involves two sections of fiber as shown in Figure 5.1. A FBG was written in a single-mode standard fiber (Corning SMF-28). A 10-W CW high-power diode laser emitting at 910-nm was used to power the FBG. The output from the 910-nm laser diode was coupled into the multi-mode fiber via a pair of 20× microscope objectives.

The coupling efficiency was approximately 23%. The low coupling efficiency was probably due to the poor beam quality of the diode laser array and slight misalignment. The power emitted by the 910-nm laser diode was controlled by a current source and the output power was confirmed by a Scientech 361 power meter. The multimode fiber (100/140) was fusion spliced to the single-mode fiber (9/125) containing the grating using a fusion splicer (Ericsson FSU995), as shown in Figure 5.2(a). The spacing between the junction and the FBG was kept at five millimeters for each of the experiments.

A uniform silver film with a resistivity of 2.2 Ω/cm was plated on the FBG section of the fiber. The coated section was approximately 5-mm from the spliced junction. The thermal expansion coefficient for silver is 5.5×10^{-6}/K in contrast to 0.66×10^{-6}/K for silica glass. The 910-nm optical energy propagating in the multimode fiber leaked into the cladding of the single-mode fiber through the spliced junction. It was estimated that most of the 910-nm light was lost within a 20-cm section starting from the fusion splice junction (Figure 5.2(b)). The leaking light was subsequently absorbed by the silver coating to raise the temperature of the FBG and shift the resonance wavelength. The reflection spectrum of the grating was monitored using an optical spectrum analyzer (OSA) and an amplified spontaneous emission (ASE) broadband source via a circulator.

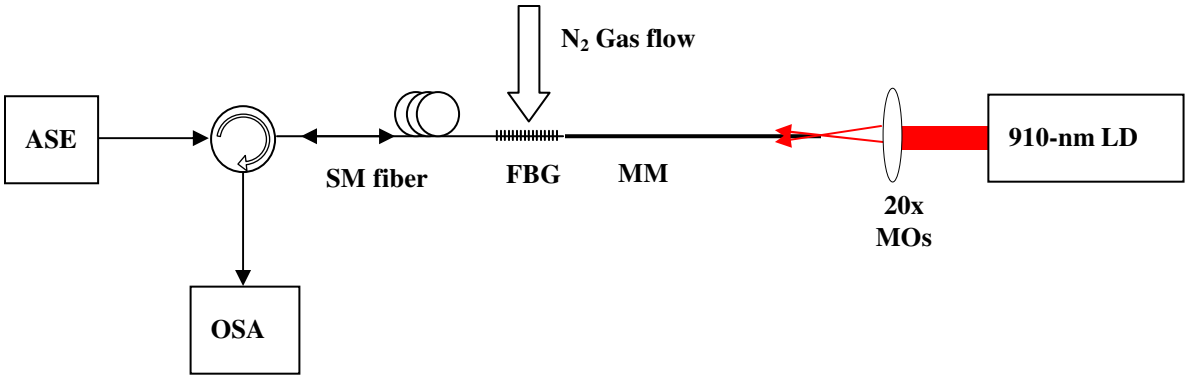

Figure 5.1: Experimental setup of a FBG flow sensor in a single-mode (SM) Fiber powered by in-fiber light.

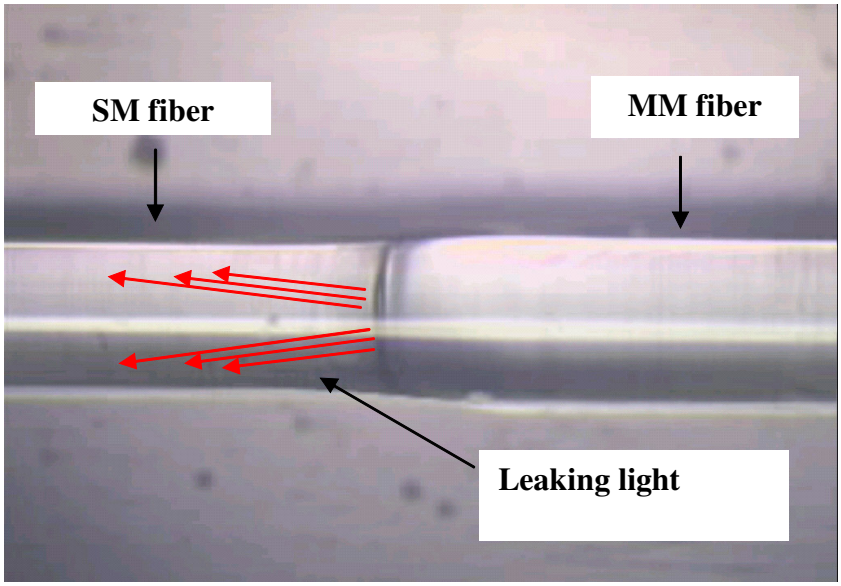

(a)

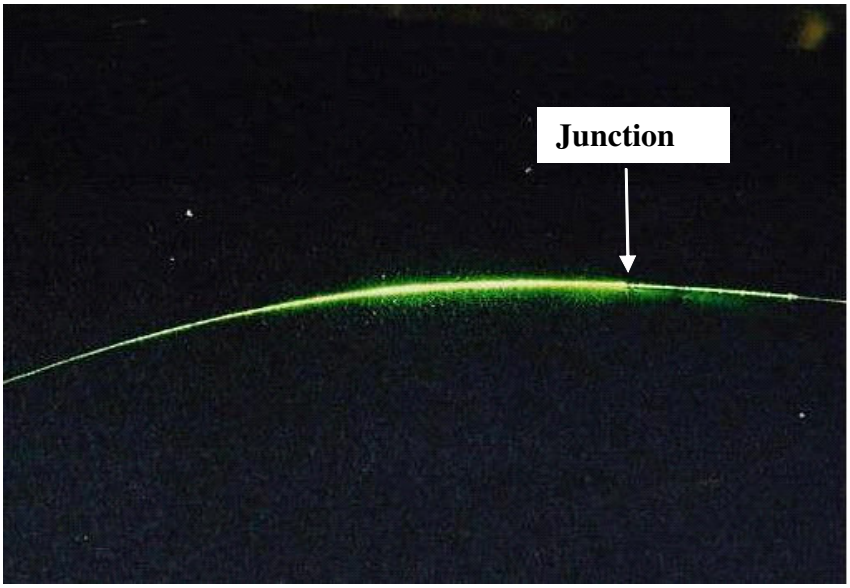

(b)

Figure 5.2: (a) Optical microscope picture of the junction between a standard 125-μm single-mode (SM) fiber and a 100-μm core/ 140-μm diameter multimode (MM) fiber. Note that the metal coating has been removed from the grating section of the fiber. (b) Photograph of green laser light leaked from the single-mode fiber cladding due to the mode mismatch.

The apparatus which applied the nitrogen gas to the sensor see Figure 5.3, consisted of a PVC pipe with an 11-mm internal diameter that was connected to a calibrated flow meter and a nitrogen tank. The pipe was held a centimeter above the grating. The gas flow direction is perpendicular to the fiber grating shown in Figure 5.1. The flow meter had a measurable range of 1 liter/min to 15 liter/min with a resolution of 1 l/min. This was converted to a measurable flow velocity ranging from 0.17 m/s to 2.63 m/s.

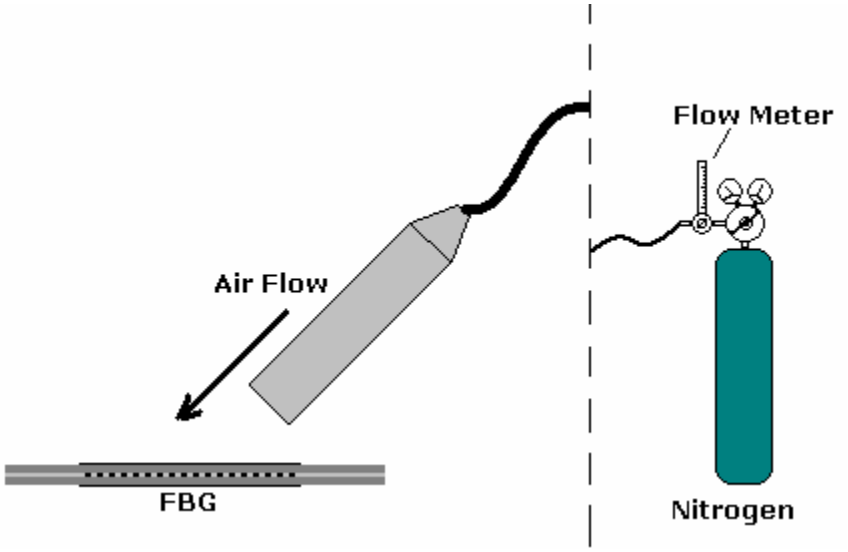

Figure 5.3: Nitrogen gas flow apparatus setup

5.3 EXPERIMENTAL RESULTS

The first set of flow experiments used a short and strong (>99% reflectance) 5-mm grating with a center wavelength λ_B of 1554.9-nm. Assuming that the 910-nm power light had a constant loss coefficient as it propagated into the single-mode fiber cladding, it was estimated that approximately 10% of the diode laser light was leaked out from the 5-mm FBG section and was absorbed by the metal coating. Without the presence of N_2 flow, 384-mW of laser power from

the 910-nm diode (40 mW absorbed by the metal coating) red shifted the resonance wavelength of the FBG by 3.3-nm to 1558.2 nm as shown in Figure 5.4. Since the silver coating has a much larger thermal expansion coefficient than that of silica, there is difficulty in predicting the exact temperature increase during the heating process.

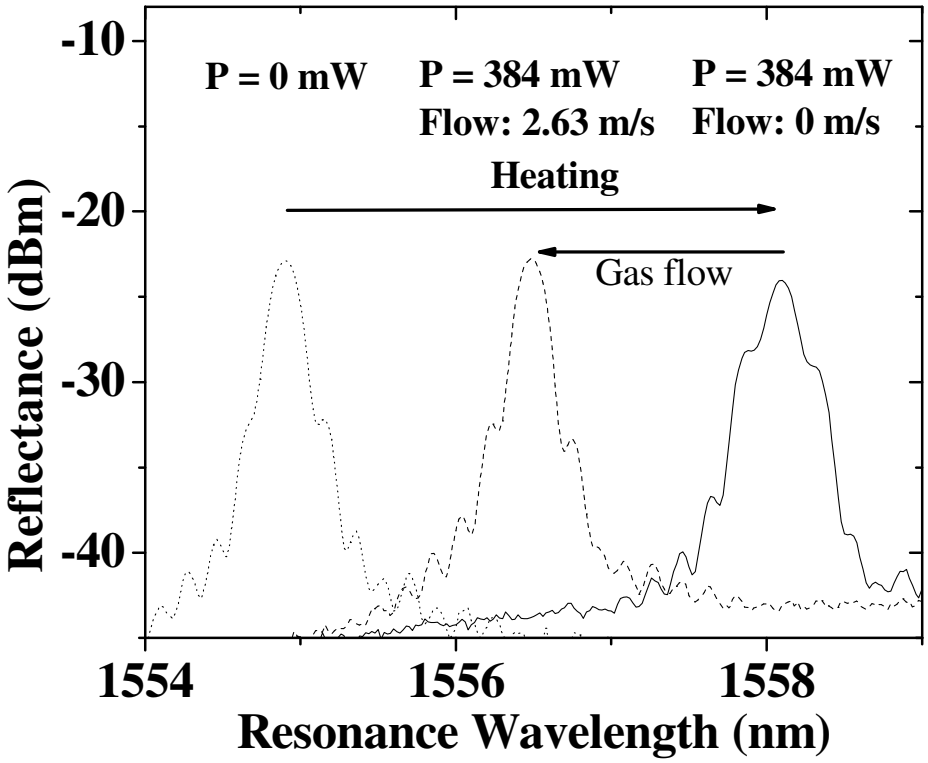

Figure 5.4: The resonance wavelength response of a heated 5-mm FBG with and without the presence of 2.63 m/s of air flow, powered by 384-mW of in-fiber diode laser light. The spectral response of the unheated FBG is also shown in the figure.

Short 5-mm FBGs were deliberately chosen in this experiment to avoid spectral distortion due to the non-uniform light absorption profile. This was confirmed in Figure 5.4, as the spectrum of the FBG was not significantly widened during the self-heating. The settling temperature and the measurement sensitivity of the FBG device can be adjusted by changing the input laser power.

When the 910-nm high-power laser is turned off, the FBG can serve as a temperature sensor for ambient gas, while the resonance wavelength will not be noticeably affected by the presence of gas flow. When the 910-nm laser is turned on, the introduction of the air flow increases the heat removal rate from the self-heated FBG device and reduces the temperature of the FBG sensor. This again was registered by the resonance wavelength shift. Shown in Figure 5.4, a 2.63 m/s N_2 flow rate led to a 1.68-nm blue shift of the resonance wavelength from that of the heated FBG without N_2 flow applied. This resonance wavelength shift can be calibrated and used to measure the flow velocity for gases.

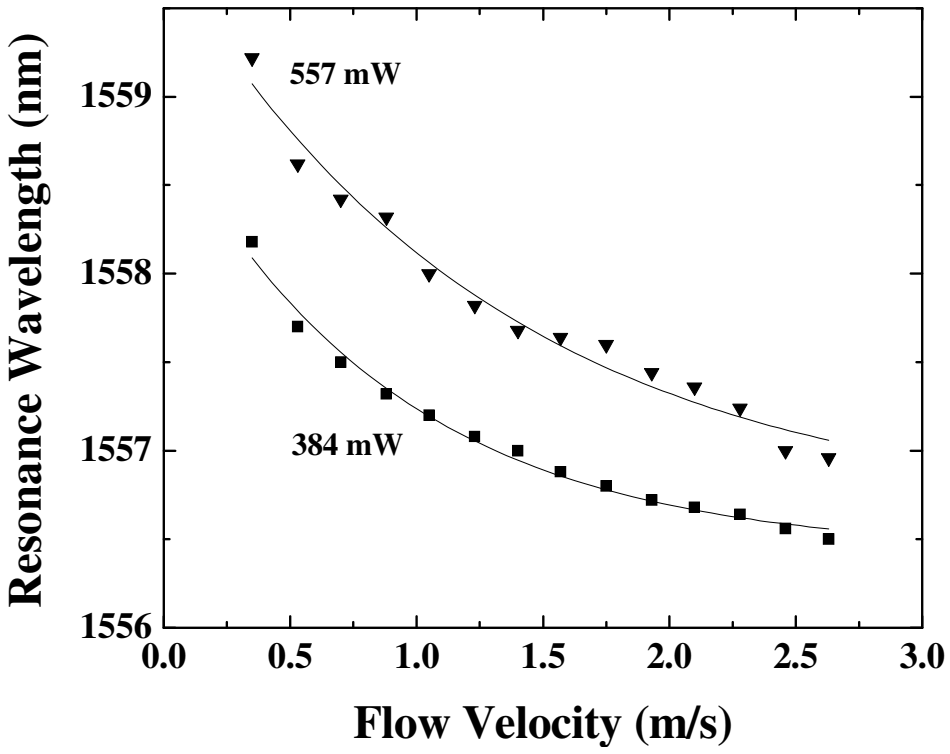

Figure 5.5: The resonance wavelength shift of a 5-mm uniform FBG subjected to various flow velocities at two distinct input laser powers of 384-mW and 557-mW.

Figure 5.5 shows the resonance wavelength shifts of the 5-mm FBG as a function of flow velocity at two input diode laser powers of 384-mW and 557-mW. The resonance wavelength shifts closely follow a simple exponential decay function versus the N_2 flow velocity. The sensitivity of the FBG flow sensor depends on the input laser power. The overall resonance wavelength shifts at a flow velocity of 2.63 m/s are 1.68-nm and 2.26-nm for the input laser powers of 384 mW and 557 mW, respectively. A 45% increase in laser power resulted in a 35% increase in the flow sensor's responsivity. The minimum flow velocity measured in this experiment was 0.35 m/s.

The flow measurements were also carried out in longer FBGs. Since the 910-nm light energy leaking out from the fiber cladding falls off exponentially with distance, a temperature gradient is created in longer FBGs. The temperature gradient non-uniformly chirps the reflection spectrum of the FBG. An example is shown in Figure 5.6. At an input of 442-mW from the 910-nm diode laser, the reflection spectrum of a 1.7-cm FBG centered at 1548.3-nm was non-uniformly widened up to 5.6 nm. A smaller reflection peak was formed at 1554.2 nm, while the original reflection peak was also slightly shifted from 1548.3 nm to 1548.6 nm. The wavelength difference between the two reflection peaks was regarded as the spectral width of the heated grating. By adjusting the coating composition and profiles using selective coating or laser ablation, it is possible to control the temperature gradient in the uniform FBG to produce chirped gratings with an arbitrary reflection spectral profile.

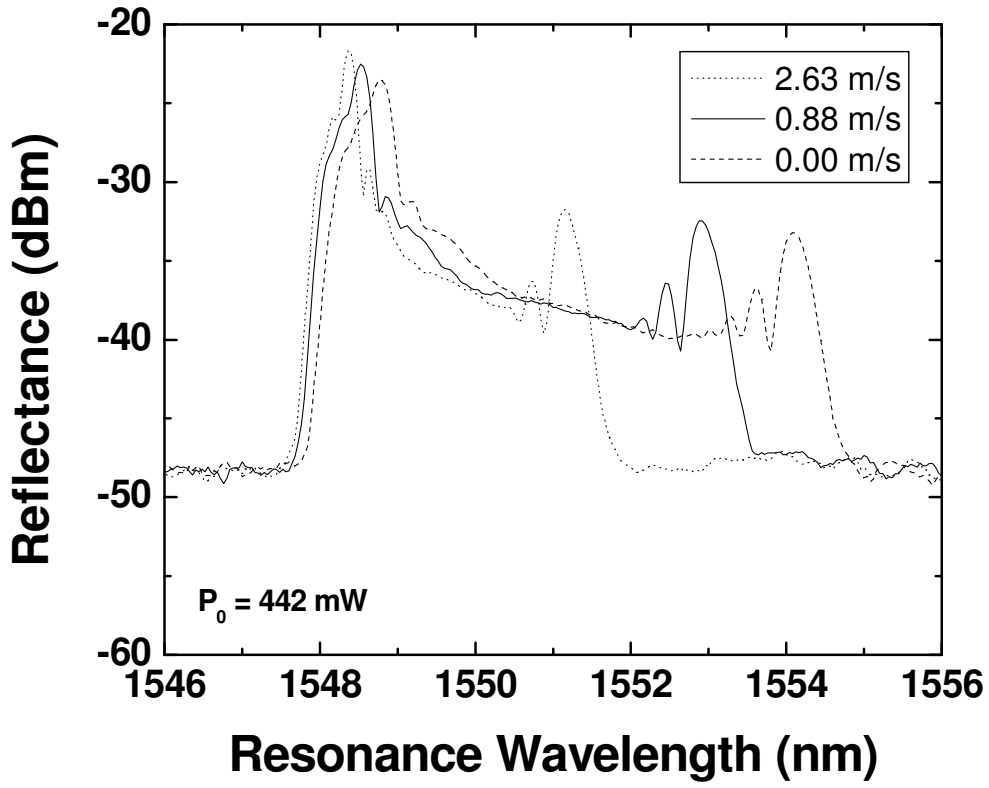

Figure 5.6: The Spectral response of a heated 1.7-cm uniform FBG at three different flow velocities of 0.00 m/s, 0.88 m/s, and 2.63 m/s. The grating was heated by 442 mW of in-fiber diode laser light.

When the 910-nm laser was turned on, the introduction of the gas flow increased the heat removal rate from the self-heated chirped FBG device, which decreased the temperature and reduced the spectral width. The reduction of the reflection peak width was then calibrated to the gas flow rate. Figure 5.6 shows the spectral evolution of a self-heated 1.7-cm uniform FBG under 0.88 m/s and 2.63 m/s flow velocities, respectively.

Figure 5.7 shows the spectral width of a self-heated 1.7-cm FBG as a function of flow velocity for two input laser powers of 345-mW and 442-mW, respectively. The spectral widths of the self-heated FBG decrease exponentially with the increase of the flow velocity for both

input laser powers. Similar to the short FBG case, the higher input laser power results in a larger response of the FBG sensor under the same gas flow velocity.

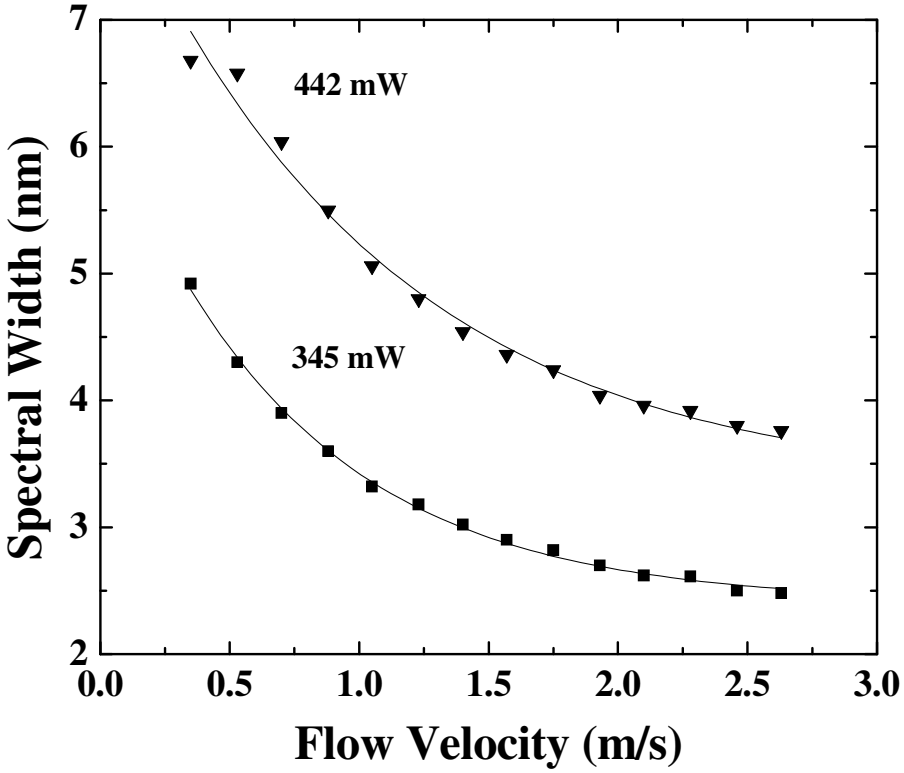

Figure 5.7: The Spectral response of a heated 1.7-cm FBG under various flow velocities. The FBG flow sensor was heated by 910nm in-fiber diode laser light at two input laser powers of 345 mW and 442 mW.

The overall change in width for the 1.7-cm uniform grating at a laser input power of 345-mW and 442-mW was 2.44-nm and 2.92-nm, respectively. A 28% increase in laser power resulted in a 20% increase in the flow sensor responsivity. The minimum flow velocity measured was found to be 0.35 m/s as well, which corresponds to a 0.38 liter/min flow rate in standard ¼ inch tubing (ID of 4.8 mm). This sensitivity is comparable to the MEMS-based flow sensor [42-45, 47].

The FBG flow sensor can also operate at a variable power mode. At this mode, the flow velocities were calibrated by increasing the input laser power to maintain the self-heated FBGs resonance wavelength or spectral width. The calibration results for a 1.7-cm uniform grating are shown in Figure 5.8(a). In these measurements, a 1.7-cm uniform FBG was initially heated by 152-mW and 325-mW input laser power respectively. The power increase needed to maintain the spectral widths were calibrated against different flow velocities. In the variable power mode, linear responses were found for both initial input laser powers of 152-mW and 325-mW. A 40% larger response was found for the larger 325-mW input power than that for the 152-mW input laser power. Figure 5.8(b) shows the measurement results for a short and strong 5-mm FBG operated under the variable power mode. The initial laser powers of 538-mW, 384-mW, and 249-mW were used to heat the FBG and pre-set the resonance wavelength. In all three cases, the laser powers needed to maintain the pre-set resonance wavelength of the heated gratings follow linear functions with the flow velocity. The 120% increase of the initial laser power from 249-mW to 538-mW led to a 120% increase of the sensor responsivity from 110 mW/(m/s) to 240 mw/(m/s).

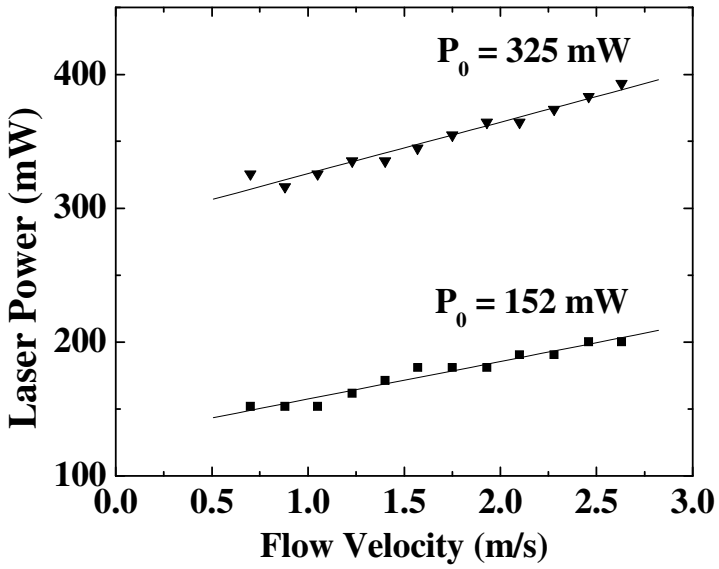

(a)

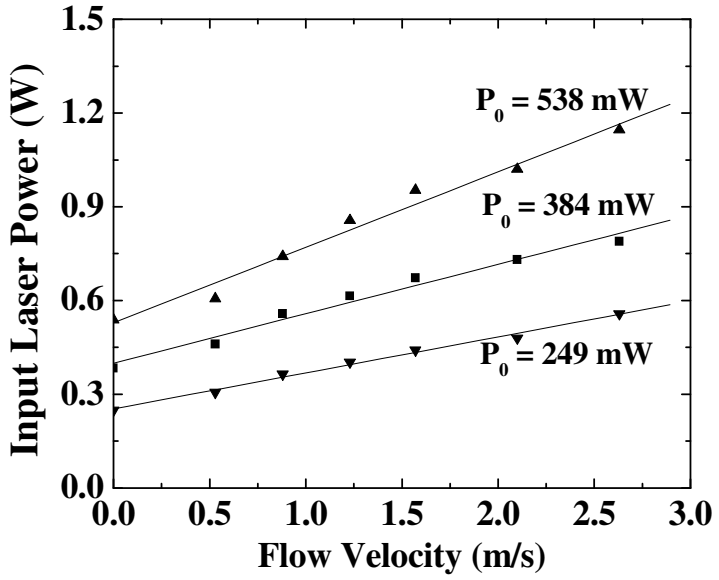

(b)

Figure 5.8: (a) The 910nm in-fiber diode laser power needed to maintain a constant spectral width for a 1.7 cm uniform FBG at various flow velocities. The initial power was set at 152-mW and 325-mW, respectively. (b) The 910nm in-fiber diode laser power needed to keep a constant spectral width for a 5-mm Short strong FBG at various flow velocities. The initial powers were set at 249-mW, 384-mW, and 538-mW.

5.4 DISCUSSION

The minimum measurable flow velocity of the self-heated flow sensor is 0.35 m/s, which is comparable to or better than most of the MEMS-based flow sensors[42-45, 47]. This minimum measurable flow velocity can be further improved by increasing the thermal contact between the grating and the surrounding fluid. Power consumption for the flow sensor demonstrated in this work is between 50 to 500 mW, which is approximately five times larger than that of MEMS-based flow sensors. This is due to the poor efficiencies in optical absorption and fiber optical coupling. By improving both efficiencies, the power consumption can be reduced to less than 40 mW for a 0.5-cm grating for effective sensor operation, which brings no power penalty to the fiber-based flow sensor in comparison to the MEMS based flow sensors. Power efficiency and device sensitivity can be further improved by using a self-heated Bragg grating in polymer fibers. Fiber Bragg gratings in polymer fibers have been demonstrated to have an over twenty-fold temperature sensitivity due to a much larger thermo-optic and thermal expansion coefficient than that of silica fibers[18].

The response time of the optically powered FBG was observed while the heated FBG's resonance wavelength shifted 1 nm from the origin when a stable input laser power was applied. The time constant, while the optical-powered FBG shifted over a range of 0.73 nm, was estimated to be less than 0.5 seconds, which is similar to FBGs tuned by electric heaters [13]. This response time was faster than resistor film heaters [17, 46] but slower than MEMS thermal sensors. The sensor response time can be improved by reducing the thermal mass of the fiber grating using chemical etching.

In conclusion, this chapter presents a novel dual function fiber grating sensor for both temperature and flow measurement. Using the optical power delivered by the optical fiber itself, a self-heated fiber Bragg grating sensor was used to measure gas flow with a minimum measurable flow velocity of 0.35 m/s. Light within optical fiber can be used for both signal and power delivery without the need of external electrical cabling, which enables the device to be both cost effective and durable.

6.0 CONCLUSION

This work presented in this thesis demonstrated a new class of active in-fiber optical components that can be directly powered by in-fiber light. On-fiber energy conversion coatings convert the light energy into thermal energy directly on the fiber. The sensitivity, trigging time, responsivity, dynamic range, and operational frequency for each fiber component can be adjusted, switched, and reset via the optical fiber to accommodate new network topologies and to adapt to the surrounding media for active sensing.

Extensive information has been presented regarding an active fiber Bragg grating flow sensor powered by in-fiber light, which had a minimum measurable flow velocity of 0.35 m/s. The active fiber Bragg grating flow sensor was comparable to most other fiber optic and MEMS based flow sensors, but with one common advantage of not being powered or controlled by remote systems via electrical wiring.

6.1 SUMMARY

Tuning of fiber Bragg gratings by in-fiber diode laser light has been presented. By sending light down a multimode fiber fusion spliced to a single mode fiber leakage into the cladding of the single mode fiber occurs. By writing a FBG into the core of the single mode fiber and surrounding the device with a light absorbing coating the light traveling down the cladding of the single mode fiber will be absorbed into the coating and raise the temperature of the FBG accordingly, thus modifying the index profile. Spectral widening of a 1.7-cm grating and

spectral shifting of a 5-mm grating has been reported in heated uniform gratings with a spectral widening of 6 nm at a laser power of 250 mW and a spectral shift of 4.9 nm at a laser power of 130 mW, respectively. Heating a 1.7-cm uniform grating with 0.8 watts of laser power resulted in a 6-nm wavelength shift of the grating or 7.5-pm/mW. Linear chirped gratings heated by in-fiber light have been shown to have spectral compression from 8-nm to 4-nm. By modifying the local light absorber surrounding the gratings novel devices can be created. Chen *et al.* demonstrated a dynamic fiber notch filter in a linear chirped FBG, where the strength of the filter was determined by the input laser power[16].

Based on the concept of tuning by in-fiber light an active fiber Bragg grating temperature and flow sensor based on hot wire anemometry was developed. Flow sensors were developed using 17-mm and 5-mm gratings, so that the amount of flow could be related either spectral widening or spectral shift of the Bragg spectra. With applied nitrogen flow ranging from 0.35 m/s to 2.63 m/s the reflected spectrum of the 17-mm grating widened 2.92 nm with an applied laser power of 442 mW. With the same nitrogen flow range the spectral shift of the 5-mm was 2.26 nm with an applied laser power of 557 mW. By measuring the spectral shift or widening of a grating the flow velocity of the nitrogen can be determined from the exponential relationship. Another method for interrogating the flow velocity was by relating the amount of power needed to keep the reflection spectra from shifting or widening as the flow velocity was changed, which results in a linear relationship with constant slope. Also, when the laser power is completely shut off the flow sensor acts as a temperature sensor for the surrounding medium.

A dual function fiber Bragg grating sensor powered by in-fiber diode laser light has be demonstrated and is comparable to other optical and MEMS based flow sensors. Considering the long lifetime of diode lasers, energy provided by high-power diode lasers through a low-loss

fiber is not only efficient, but economical. Together with low cost in-fiber sensor technology, such as fiber Bragg gratings, active sensing powered by in-fiber light should have a significant impact on the fiber sensor industry. The work presented in this thesis has resulted in the following publications:

Journal Papers:

[1] K. P. Chen, L. J. Cashdollar, and X. Wu, "Controlling Fiber Bragg Grating Spectra with In-Fiber Diode Laser Light," *IEEE Photon. Tech. Lett*., vol. 16, no. 8, pp. 1897-1899, 2004.

[2] Cashdollar, L.J. and K.P. Chen, "Fiber Bragg Grating Flow Sensor Powered by In-Fiber Light, Sensors Journal, IEEE, 2004, accepted: subjected to minor revision.

Conference Papers:

[1] K. P. Chen, and L. Cashdollar, "Tuning Fiber Bragg Grating with In-Fiber Light," OSA TOPS 71, Bragg Gratings, Photosensitivity, and Poling in Glass Waveguides, OSA Tech. Digest, (OSA, Washington DC, 2003), paper MD8.

[2] K. P. Chen and L. Cashdollar, "Fiber-Optical Tunable Filters Powered by In-Fiber Light" Conference on Lasers and Electro-optics (CLEO'04), Tech. Digest, (OSA Washington DC, 2004), paper CWD3.

[3] K. P. Chen, and L. Cashdollar, "In-fiber Light Powered Active Fiber Components Technology," submitted to SPIE Photonics North, 2004.

6.2 FUTURE WORK

The current tuning mechanism powered by in-fiber laser light presented in Section 4.2 can only support one active fiber component without a substantial loss in the amount of laser power delivered to each device, due to exponential loss in light energy along the length of the fiber. Dr. Kevin P. Chen has developed a scheme so that multiple FBGs can be placed on the same length of fiber to create a grating network, such as an active fiber sensor array. Using a double-cladding specialty fiber, the optical power source can be launched together with the 1.55-μm sensing source, from the same side of the fiber, to power a large grating array, see Figure 6.1.

The proposed fiber is a fluorine-doped double-cladding polarization-maintaining fiber with a bending insensitive ellipse core, as shown in Figure 6.2(a). The inner elliptical core has dimensions of 5 μm by 8 μm and is doped with germanium and boron to achieve a numerical aperture of 0.16, which is higher than 0.13 of standard telecommunications fiber, so as to achieve less bending loss.

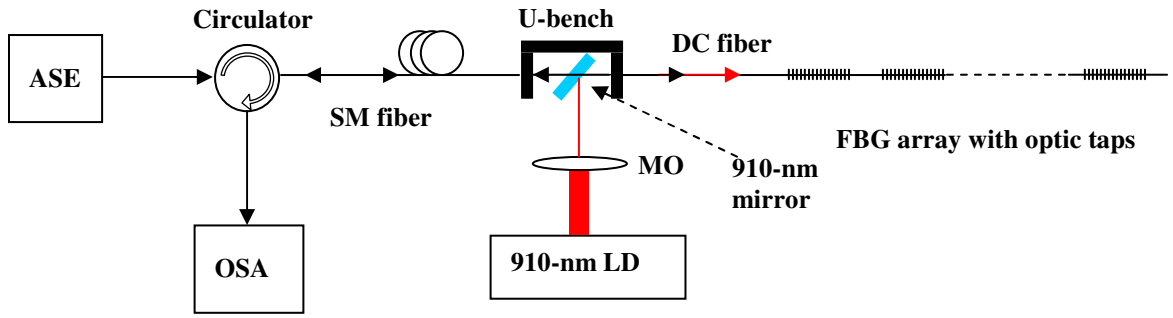

Figure 6.1: Proposed fiber Bragg grating sensor array in the double-cladded (DC) fiber powered by light. Light from a high-power laser diode (LD) was focused by a microscope objective (MO) and coupled into the DC fiber sensor array using a U-bench.

Also, the elliptical core is polarization maintaining and has a beat length of less than 4 mm at 1550 nm to ensure high sensitivity and to reduce polarization phase noise. The inner cladding is a 105-μm diameter pure fused silica, which has a high damage threshold and is ideal for high-power laser light delivery. The outer cladding is 10-μm thick and consists of fused silica glass doped with 3% fluorine, which creates an index contrast of 0.3% between the two glass layers and corresponds to a NA of 0.13. This leaves the total diameter of the specialty fiber at 125-μm which matches the diameter of single mode standard telecommunications fiber. Both the outer and inner cladding are transparent to UV light at 248-nm, so that a fiber Bragg grating can be written into the core uniformly without being affected by either of the claddings.

The 10-μm depth of the outer cladding allows for optical taps to be created by ion implantation, so that laser light traveling down the inner cladding can leak out to heat a metallic coating. See Figure 6.3 for a diagram of the optical tap, FBG, and leaking light. The optical taps are needed to allow the laser light to power the tuning mechanisms of each of the sensors along the length of the fiber network.

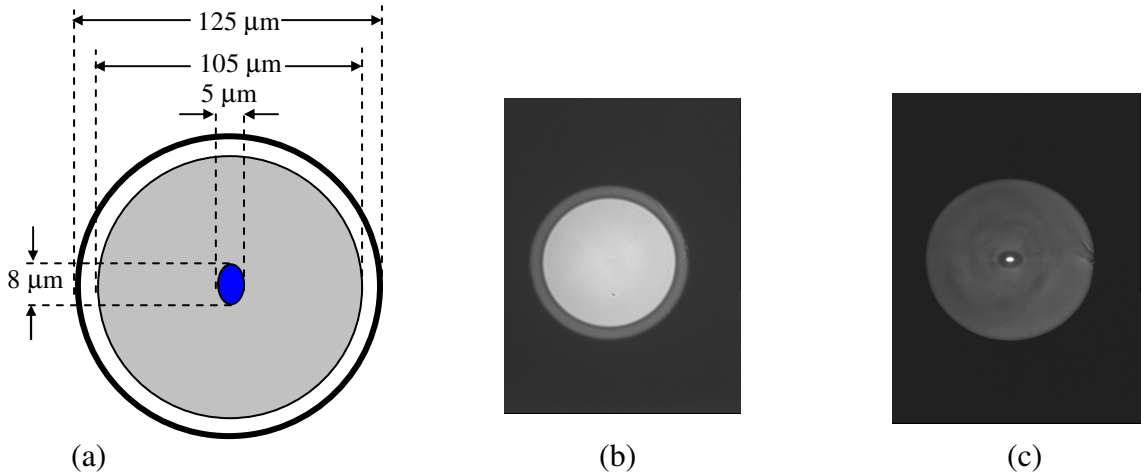

Figure 6.2: (a) sketch of the double-cladding fiber, which consists of a combination of (b) the 100/125-µm fluorine-doped multimode fiber and (c) elliptical core bending insensitive fiber. Both fibers shown in (b) and (c) are provided by StockerYale Inc. (Salem, NH).

Ion irradiation is an ideal method in which to produce an optical tap in the proposed fiber structure. Optical devices such as ion-implanted waveguides and long-period fiber gratings have been demonstrated in various silica glasses and fibers[49, 50]. The magnitude and location of an index change in an optical fiber can be precisely controlled by the selected ion species, ion energy, and total ion dose so that no signal loss will be created for the sensing signal passing thought the elliptical core. By choosing proper ion species, energy, and dose, up to 1.1×10^{-2} index change could be produced in fused silica with a penetration depth $>10\,\mu m$. An index change of 5×10^{-3} to 1×10^{-2} through the 10-μm -thick outer cladding will be sufficient to release the optical energy from the proposed double-clad fiber.

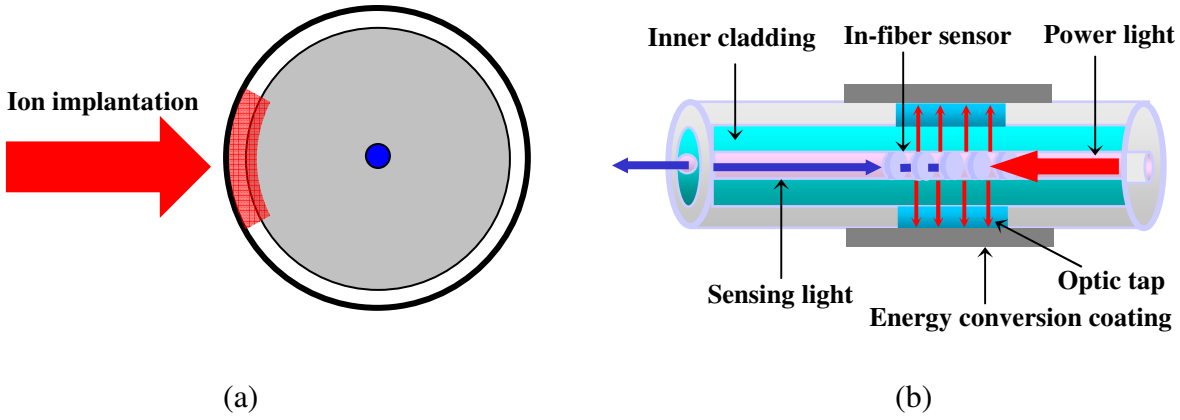

Figure 6.3: (a) Formation of an optical tap in a double clad fiber by ion implantation. (b) Diagram of a double clad fiber showing light passing through optical taps and being absorbed in the energy converting coating to modify the properties of the FBG.

Currently the active fiber components demonstrated in the work presented in this thesis are all driven by thermal energy converted from the in-fiber light. In the future, research will focus on developing novel fiber components that convert the in-fiber optical energy into mechanical, electrical, and magnetic energy, which will bring to light a wide range of

applications. One such approach involves photomechanical actuation that is based on thermal polymerized liquid crystal coatings. Polymer membranes which contain light sensitive molecules undergo rapid contraction or expansion when radiated by weak polarized light. Yu *et al.* has shown that a liquid crystal membrane containing azobenzene chromeophore can be repeatedly bent using weak laser radiation without any apparent signs of fatigue[51]. By using linearly polarized light mechanical bending of the membrane can be precisely controlled. By coating a photomechanical membrane directly to the in-fiber Bragg grating in-fiber laser light can be converted into mechanical energy rather than thermal energy.

BIBLIOGRAPHY

1. Hill, K.O., et al., *Photosensitivity in optical fiber waveguides: Application to reflection filter fabrication.* Applied Physics Letters, 1978. **32**(10): p. 647-649.

2. Lehman, R.L. *Developments in fiber optic sensor design*. in *Electronic Components and Technology Conference, 1990. Proceedings., 40th*. 1990.

3. Limberger, H.G., et al., *Efficient miniature fiber-optic tunable filter based on intracore Bragg grating and electrically resistive coating.* Photonics Technology Letters, IEEE, 1998. **10**(3): p. 361-363.

4. Doyle, A., et al., *FBG-based multi-channel low dispersion WDM filters.* Electronics Letters, 2002. **38**(24): p. 1561-1563.

5. Yeom, D.I., H.S. Park, and B.Y. Kim, *Tunable narrow-bandwidth optical filter based on acoustically modulated fiber Bragg grating.* Photonics Technology Letters, IEEE, 2004. **16**(5): p. 1313-1315.

6. Nykolak, G., et al., *All-fiber active add-drop wavelength router.* Photonics Technology Letters, IEEE, 1997. **9**(5): p. 605-606.

7. Feng, K.-M., et al. *Tunable nonlinearly-chirped fiber Bragg grating for use as a dispersion compensator with a voltage-controlled dispersion*. in *Optical Fiber Communication Conference and Exhibit, 1998. OFC '98., Technical Digest*. 1998.

8. Rogers, J.A., et al., *Distributed on-fiber thin film heaters for Bragg gratings with adjustable chirp.* Applied Physics Letters, 1999. **74**(21): p. 3131-3133.

9. Kersey, A.D. *Multiplexed Bragg grating fiber sensors*. in *Lasers and Electro-Optics Society Annual Meeting, 1994. LEOS '94 Conference Proceedings. IEEE*. 1994.

10. Rao, Y.-J., et al., *In-fiber Bragg-grating temperature sensor system for medical applications.* Lightwave Technology, Journal of, 1997. **15**(5): p. 779-785.

11. Iida, T., K. Nakamura, and S. Ueha. *A microphone array using fiber Bragg gratings*. in *Optical Fiber Sensors Conference Technical Digest, 2002. OFS 2002, 15th*. 2002.

12. Zhang, Y., et al., *High-sensitivity pressure sensor using a shielded polymer-coated fiber Bragg grating.* Photonics Technology Letters, IEEE, 2001. **13**(6): p. 618-619.

13. Guan, B., H. Tam, and S. Liu, *Temperature-Independent Fiber Bragg Grating Tilt Sensor.* Photonics Technology Letters, IEEE, 2004. **16**(1): p. 224-226.

14. Lopez-Higuera, J.M., et al. *Simultaneous temperature and acceleration optical fiber sensor system for large structures monitoring*. in *Lasers and Electro-Optics Society 2000 Annual Meeting. LEOS 2000. 13th Annual Meeting. IEEE*. 2000.

15. Othonos, A. and K. Kalli, *Fiber Bragg Gratings, Fundamentals and Applications in Telecommunications and Sensing*. 1999, Norwood, USA: Artech House Publishing.

16. Chen, K.P., L.J. Cashdollar, and W. Xu, *Controlling Fiber Bragg Grating Spectra with in-fiber Diode Laser Light.* Photonics Technology Letters, IEEE, 2004.

17. Buchanan, J.E.S.a.R.C., *Thermal sensor properties of cermet resistor films on silicon substrates.* Sen. Actuators A, 2001. **90**: p. 118-124.

18. Liu, H.Y., G.D. Peng, and P.L. Chu, *Thermal tuning of polymer optical fiber Bragg gratings.* Photonics Technology Letters, IEEE, 2001. **13**(8): p. 824-826.

19. Bae, J.K., et al., *Spectral shape tunable band-rejection filter using a long-period fiber grating with divided coil heaters.* Photonics Technology Letters, IEEE, 2003. **15**(3): p. 407-409.

20. Inui, T., T. Komukai, and M. Nakazawa, *A wavelength-tunable dispersion equalizer using a nonlinearly chirped fiber Bragg grating pair mounted on multilayer piezoelectric transducers.* Photonics Technology Letters, IEEE, 2000. **12**(12): p. 1668-1670.

21. Song, Y.W., et al., *40-nm-wide tunable fiber ring laser with single-mode operation using a highly stretchable FBG.* Photonics Technology Letters, IEEE, 2001. **13**(11): p. 1167-1169.

22. Goh, C.S., et al., *Wavelength tuning of fiber Bragg gratings over 90 nm using a simple tuning package.* Photonics Technology Letters, IEEE, 2003. **15**(4): p. 557-559.

23. Kashyap, R., *Fiber Bragg Gratings*. 1999, San Diego, CA: Academic Press.

24. Metlz, G., W.W. Morey, and W.H. Glenn, *Formation of Bragg gratings in optical fibers by a transverse holographic method.* Optics Letters, 1989. **14**(15): p. 823-825.

25. Kashyap, R., et al., *All-fibre narrowband reflection gratings at 1500 nm.* Electronics Letters, 1990. **26**(11): p. 730-732.

26. Chen, K.P., P.R. Herman, and R. Tam, *Strong fiber Bragg grating fabrication by hybrid 157- and 248-nm laser exposure.* Photonics Technology Letters, IEEE, 2002. **14**(2): p. 170-172.

27. Atkins, R.M., V. Mizrahi, and T. Erdogan, *248 nm induced vacuum UV spectral changes in optical fibre preform cores: support for a colour centre model of photosensitivity.* Electronics Letters, 1993. **29**(4): p. 385-387.

28. Othonos, A., *Fiber Bragg gratings.* Rev. Sci. Instrum., 1997. **68**(12): p. 4309-4341.

29. Chen, K.P., *Gratings, Photosensitivity, and Poling in Silica Optical Waveguides with 157-nm F2 Laser Radiation*. 2002, University of Toronto: Toronto.

30. C. Fiori, R.A.B.D., *Evidence for a wide continuum of polymorphs in a-SiO2.* Phys. Rev. B (APS), 1986. **33**(4): p. 2972 - 2974.

31. Du, W., X. Tao, and H.-Y. Tam, *Temperature independent strain measurement with a fiber grating tapered cavity sensor.* Photonics Technology Letters, IEEE, 1999. **11**(5): p. 596-598.

32. Du, W.-C., X.-M. Tao, and H.-Y. Tam, *Fiber Bragg grating cavity sensor for simultaneous measurement of strain and temperature.* Photonics Technology Letters, IEEE, 1999. **11**(1): p. 105-107.

33. Malo, B., et al., *Point-by-point fabrication of micro-Bragg gratings in photosensitive fibre using single excimer pulse refractive index modification techniques.* Electronics Letters, 1993. **29**(18): p. 1668-1669.

34. Rao, Y.-J., *In-fiber Bragg Grating sensors.* Measurement Science and Technology, 1997. **8**: p. 355-375.

35. Hill, K.O., et al., *Bragg gratings fabricated in monomode photosensitive optical fiber by UV exposure through a phase mask.* Applied Physics Letters, 1993. **62**(10): p. 1035-1037.

36. GSI-Lumonics, *PulseMaster PM-800 User's Manual*. 2000, GSI Lumonics: Canada.

37. Barber, D.A. and N.H. Rizvi, *Practical study of the effects of exposure conditions on the quality of fiber Bragg gratings written with excimer and argon-ion lasers.* Proc. SPIE, 2003. **4941**: p. 16-25.

38. Zhang, Q., et al., *Tuning Bragg wavelength by writing gratings on prestrained fibers.* Photonics Technology Letters, IEEE, 1994. **6**(7): p. 839-841.

39. Dabarsyah, B., et al., *Adjustable dispersion-compensation devices with wavelength tunability based on enhanced thermal chirping of fiber Bragg gratings.* Photonics Technology Letters, IEEE, 2003. **15**(3): p. 416-418.

40. Wu, J. and W. Sansen, *Electrochemical time of flight flow sensor.* Sen. Actuators A, 2002. **97-98**: p. 68-74.

41. Lim, J., et al., *DP flow sensor using optical fiber grating.* Sen. Actuators A, 2001. **92**: p. 102-108.

42. Oda, S., et al., *A silicon micromachined flow sensor using thermopiles for heat transfer measurements.* IEEE Tran. Instrum. Meas., 2003. **52**: p. 1155-1159.

43. Kaltsas, G., A.A. Nassiopoulos, and A.G. Nassiopoulou, *Characterization of a silicon thermal gas-flow sensor with porous silicon thermal isolation.* IEEE Sensors, 2002. **2**: p. 463-475.

44. Hung, S.T., S.C. Wong, and W. Fang, *The development and application of microthermal sensors with mesh-membrane supporting structure.* Sen. Actuators A, 2000. **84**: p. 70-75.

45. Gamage, S.K., N. Okulan, and H.T. Henderson, *A silicon thermal astable multivibrator for flow and temperature sensing.* IEEE Tran. Electron. Devices., 2002. **49**: p. 2355-2358.

46. Dominguez, M., et al., *Low-cost thermal Sigma-Delta air flow sensor.* IEEE Sensors, 2002. **2**: p. 453-462.

47. Svedin, N., E. Kalvesten, and G. Stemme, *A new edge-detected life force flow sensor.* J. MEMS, 2003. **12**: p. 344-354.

48. Nemoto, T., et al., *An Optical Fiber Flow Speed Sensor of Increased Sensitivity.* Electrical Engineering in Japan, 1998: p. 1-8.

49. Radhakrishnan, S., H. Solak, and A. Lal, *In-channel microbeam flow sensor using drag forces.* MircoTAS2001, 2001: p. 179 - 180.

50. Bracio, B.R., et al., *A smart thin-film flow sensor for biomedical applications.* Proc of the 22nd Annual EMBS Conference, 200: p. 2800 - 2801.

51. Yu, Y., M. Nakano, and T. Ikeda, *Directed bending og a polymer film by light.* Nature, 2003. **425**: p. 145.